NSP-74-105A
Revision 1
November 1982
30.2874.2105

APPENDIX A

MONTICELLO RESPONSES TO PREVIOUS PLANT UNIQUE ANALYSIS REPORT CURRENT CONTAINMENT AND PIPING LICENSING ISSUES

nutech ENGINEERS

REVISION CONTROL SHEET

TITLE: Monticello Nuclear Generating Plant
Plant Unique Analysis Report
Volume 5, Appendix A

REPORT NUMBER: NSP-74-105A
Revision 1

R. O. Nunn/Consultant I	RON INITIALS
H. K. Fatehi/Specialist	HKF INITIALS
K. E. Parzyck/Specialist	KEP INITIALS
W. J. Steffey/Principal Engineer	WJS INITIALS
F. A. Villarreal/Engineering Analyst	FAV INITIALS
K. W. Bentin /Consultant I	KWB INITIALS
J. R. Bondre/Consultant II	HA FOR JRB INITIALS
A. S. Herlekar/Unit Supervisor	ASH INITIALS
T. I. Hsu/Senior Engineer	TIH INITIALS
J. W. Axline/Engineering Manager	JWA INITIALS
R. A. Sánchez/Unit Supervisor	RAS INITIALS
S. Y. Kun /Consultant I	SYK INITIALS
I. D. McInnes/Engineering Manager	IDM INITIALS

REVISION CONTROL SHEET
(Concluded)

TITLE: Monticello Nuclear Generating Plant
Plant Unique Analysis Report
Volume 5, Appendix A

REPORT NUMBER: NSP-74-105A
Revision 1

EFFECTIVE PAGE(S)	REV	PREPARED	ACCURACY CHECK	CRITERIA CHECK
A-ii	1	LDM	[illegible]	N/A
A-iii				
A-iv				
A-1		HA for JRB		
A-2				
A-3				
A-4				
A-5			KWB	
A-6			KWB	
A-7			KWB	
A-8		KWB	IDM	
A-9				
A-10				
A-11				
A-12				
A-13				
A-14		KWB	IDM	
A-15		TCH	SYK	
A-16		TCH	SYK	
A-17		TCH	SYK	
A-18		HA for JRB		
A-19				
A-20		KWB	JAN	
A-21		KWB	IDM	
A-22		HA for JRB		
A-23				
A-24				
A-25				
A-26				
A-27				
A-28				
A-29				
A-30				
A-31				
A-32				
A-33				
A-34		KWB	KEP	
A-35				
A-36				
A-37			KEP	
A-38			IDM	
A-39				
A-40				
A-41				
A-42	1	KWB	IDM	N/A

EFFECTIVE PAGE(S)	REV	PREPARED	ACCURACY CHECK	CRITERIA CHECK
A-43	1	KWB	IDM	N/A
A-44				
A-45				
A-46				
A-47				
A-48				
A-49				
A-50			IDM	
A-51			HKF	
A-52				
A-53				
A-54				
A-55				
A-56				
A-57			HKF	
A-58			IDM	
A-59			IDM	
A-60		KWB	JAN	
A-61		ASH	JWA	
A-62				
A-63				
A-64				
A-65				
A-66				
A-67				
A-68				
A-69				
A-70			JWA	
A-71		ASH	RAS JWA	
A-72		HA for JRB	RAS JWA	
A-73			RAS JWA	
A-74				
A-75		KWB	RON	
A-76			RON	
A-77			JAN	
A-78				
A-79				
A-80				
A-81				
A-82				
A-83				
A-84				
A-85				
A-86	1	KWB	JAN	N/A

ABSTRACT

This appendix provides Monticello plant unique responses to current Mark I containment and piping licensing issues which have evolved as a result of the review of other plant unique analysis reports. It is submitted as part of the PUAR in anticipation of the applicability of these issues to the Monticello plant. The appendix is in a question-and-answer format and addresses topics in each of the five volumes of the report.

Question 1

Published acceleration drag volumes were used to determine the drag loads on sharp cornered submerged structures instead of the equivalent cylinder procedure specified in the acceptance criteria. Provide a list of structures which were treated in this manner. For the ring girder, provide specific dimensions of the structure, as well as the local acceleration and velocity for the post-chug loading condition. A copy of K. T. Patton's MS thesis from the University of Rhode Island (1965) would be useful in resolving this issue if it is available.

Response to Question 1

The alternate method for calculating acceleration drag volumes was used for the ring girder only. The ring girder was divided into the segments shown in PUAR Table 2-2.2-9 for analysis of post-chug submerged structure loads.

Post-chug submerged structure loads on the ring girder were calculated on the basis of the two nearest downcomers chugging at the maximum source strength with the downcomer phasing selected to maximize the local acceleration. Segment 7 of the ring girder experiences the highest loads, as shown in PUAR Table 2-2.2-9. Forces are calculated for the 50 frequencies and corresponding source strengths listed in PUAR Table 1-4.1-15.

The following information presents sample calculations of post-chug submerged structure loads on Segment 7 of the ring girder.

For submerged structure loads, the contribution due to velocity drag is negligible compared to acceleration drag. Figure 1-1 shows the cross-section of the ring girder at Segment 7 used for calculating the acceleration drag volume. For the flow direction shown in Figure 1-1, the ring girder is idealized as an I-beam plus a plate. The acceleration drag volume (LDR Table 4.3.4-1), V_{Total}, for this combination is:

$$V_{Total} = VOL_{(I\text{-beam})} + VOL_{(plate)} =$$

$$[4a_1c + 2bc - 2c^2 + 2.11\ \pi a_1^2]\ LA_w + \pi a_2^2 LA_w$$

Where A_w = Wall interference factor

and L = Length of the segment

For Segment 7, $A_w = 2.0$ and $L = 2.36$ feet. This results in a drag volume equal to 8.50 ft^3 for Segment 7.

For the bounding load case (two downcomers chugging out of phase), the acceleration, A_y, on Segment 7 normal to the direction of the flange for a unit source strength was calculated as 0.01784 ft/sec^2. Therefore, the force, F, for the unit source strength will be:

$$F = \frac{\rho V A_y}{g_c} = 0.294 \text{ lbs.}$$

Table 1-1 shows the results of sample calculations for the dynamic force in each frequency range from 0 to 50 Hz. Dynamic load factors are calculated corresponding to the 25.14 Hz natural frequency of the ring girder given in PUAR Figure 2-2.4-9. The dynamic force in each frequency range is summed absolutely and multiplied by a factor of 0.65 to account for randomness in phasing. The horizontal projection of the flange surface area of Segment 7 was calculated as 160.8 in^2 from the finite element model shown in PUAR Figure 2-2.4-4. Therefore, the pressure on the flange at Segment 7 of the ring girder as shown in PUAR Table 2-2.2-9 (without the FSI effect) is calculated as:

$$\text{Pressure} = \frac{0.65 \times \sum_{i=1}^{50} (F \times DLF)_i}{\text{Area of Segment 7}}$$

and is equal to 22.2 psi, as shown in Table 1-1.

As discussed earlier, the acceleration drag volume for various segments of the ring girder for the flow direction normal to the flange has been calculated for an I-section plus a plate. Overall, the submerged structure loads in the PUAR have been calculated conservatively.

The right-hand coordinate system is:

TORUS CROSS-SECTION

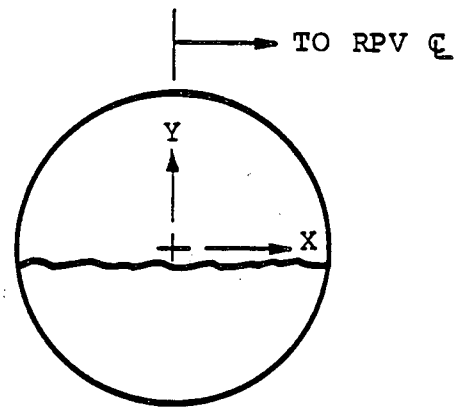

K.T. Patton's master's thesis is not available from either the University of Rhode Island or the author.

Table 1-1

DYNAMIC FORCE ON SEGMENT 7 DUE TO POST-CHUG SUBMERGED STRUCTURE LOADS

FREQUENCY (Hz)	FORCE CORRESPONDING TO AMPLITUDE AT EACH FREQUENCY (F) (lbs)	DYNAMIC LOAD FACTOR (DLF)	DYNAMIC FORCE (F x DLF) (lbs)
0-1	3.5	1.01	3.6
1-2	3.5	1.02	3.6
2-3	3.0	1.03	3.1
3-4	2.9	1.05	3.0
4-5	5.1	1.07	5.5
5-6	5.0	1.10	5.5
6-7	5.6	1.13	6.3
7-8	5.6	1.18	6.6
8-9	5.6	1.23	6.9
9-10	5.6	1.30	7.3
10-11	25.8	1.38	35.6
11-12	22.4	1.49	33.4
12-13	12.1	1.62	19.6
13-14	10.6	1.79	19.0
14-15	2.0	2.02	4.0
15-16	1.8	2.33	4.2
16-17	0.9	2.78	2.5
17-18	1.2	3.49	4.2
18-19	0.9	4.73	4.3
19-20	4.9	7.41	36.3
20-21	5.2	16.14	83.9
21-22	9.0	24.10	216.9
22-23	27.2	9.92	269.8
23-24	27.2	10.18	276.9
24-25	39.5	24.26	958.3
25-26	92.3	12.29	1134.4
26-27	111.1	7.54	837.7

Table 1-1

DYNAMIC FORCE ON SEGMENT 7 DUE TO POST-CHUG SUBMERGED STRUCTURE LOADS

(Concluded)

Frequency (Hz)	Force Corresponding to Amplitude at Each Frequency (F) (lbs)	Dynamic Load Factor (DLF)	Dynamic Force (F x DLF) (lbs)
27-28	74.1	5.64	417.9
28-29	48.0	4.21	202.1
29-30	34.3	2.15	73.7
30-31	12.7	1.83	23.2
31-32	6.3	1.65	10.4
32-33	11.1	1.49	16.5
33-34	14.9	1.36	20.3
34-35	12.5	1.26	15.8
35-36	18.2	1.20	21.8
36-37	12.3	1.12	13.8
37-38	6.2	1.13	7.0
38-39	7.2	1.21	8.7
39-40	8.6	1.51	13.0
40-41	66.1	1.45	95.8
41-42	66.1	1.33	87.9
42-43	66.1	1.36	89.9
43-44	66.1	1.54	101.8
44-45	66.1	1.95	128.9
45-46	66.1	1.30	85.9
46-47	66.1	.54	35.7
47-48	66.1	.24	15.9
48-49	66.1	.10	6.6
49-50	66.1	.07	4.6
		Total	5489.6

Total Pressure = $\frac{5489.6 \times 0.65}{160.8}$ = 22.2 psi (See page A-3 for applicable formula).

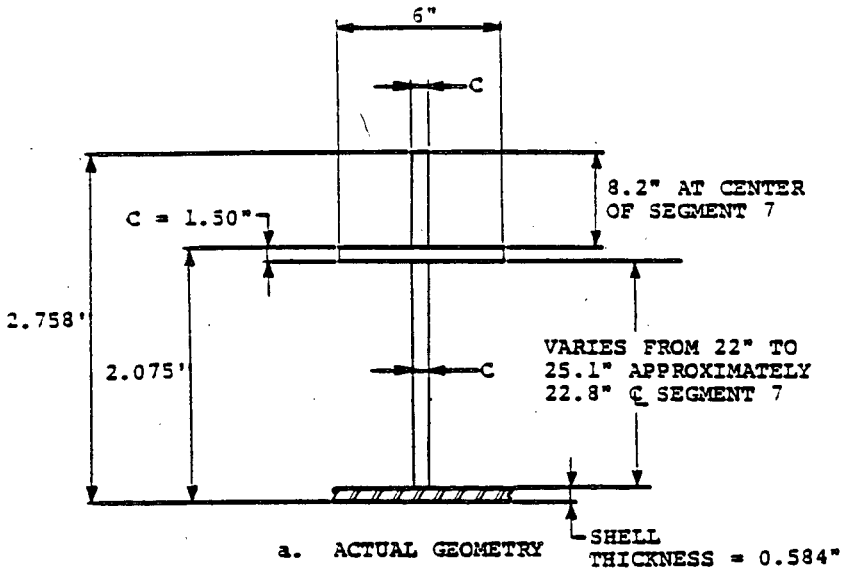

a. ACTUAL GEOMETRY

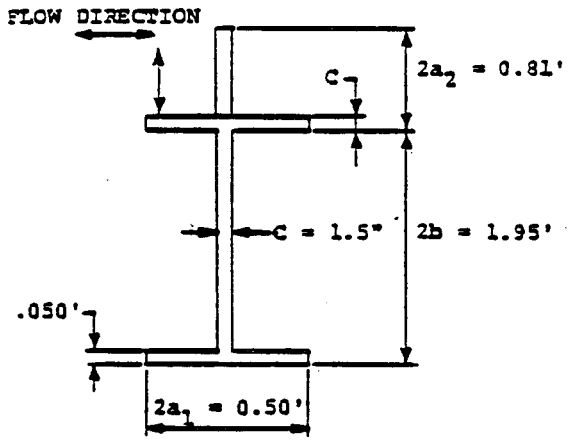

b. MODEL GEOMETRY

Figure 1-1

RING GIRDER CROSS-SECTION AT SEGMENT 7
FOR ACCELERATION DRAG VOLUME CALCULATION

nutech ENGINEERS

Question 2

A statistical basis was used to account for random phasing of the loading harmonics for condensation oscillation and chugging loadings. The random phasing approach consists of multiplying the absolute sum of the responses (i.e., the AC-accepted approach) by a scale factor determined from the FSTF data. Provide more detailed documentation for the justification of the 0.65 value of the scale factor and comment on the remaining conservatism after application of this factor for both the condensation oscillation and chugging loadings. List all loads (such as CO, post-chug, etc.) and all structures (such as torus shell, ring girder, etc.) for which the scale factor is used. In addition, provide the basis for the statement that Alternate 4 leads to a 20% increase in the loads and verify the numbers given in Table 1-4.1-4 on page 1-4.45. In particular, check the consistency of these numbers with those given in the FSTF letter report MI-LR-81-01.

Response to Question 2

The loads for which the random phasing methods were used to combine harmonic responses are:

a. DBA Condensation Oscillation Loads on the Torus Shell

b. DBA Condensation Oscillation Loads on Submerged Structures

c. Post-Chug Loads on the Torus Shell

d. Post-Chug Loads on Submerged Structures

The components of the torus and vent system affected by the above loads are identified in Monticello PUAR Tables 2-2.2-1 and 3-2.2-1.

When combining harmonic responses, NEDE-24840 recommends use of a 50% non-exceedance probability (NEP) value based on random phasing cumulative distribution function (CDF) curves as a means of providing an appropriate level of conservatism for the combined response. The approach used in the Monticello plant unique analysis (PUA) consists of multiplying the absolute sum of the harmonic responses by a scale factor of 0.65, determined from the data contained in NEDE-24840. The method estimates the response at 84% NEP with a 90% confidence level as described in Section 1-4.1.7.1 of the PUAR. This method of combining harmonic responses is more conservative than that recommended in NEDE-24840.

The scale factor of 0.65 was derived from the 14 response quantities given in Tables 6-1 through 6-3 of NEDE-24840. Ratios of the absolute sum and 84% NEP response values from these tables were calculated as shown in Table 2-1. The mean (μ) and

standard deviation (σ) values were calculated for the ratios of these 14 responses. Using a Gaussian (normal) distribution, the tolerance limit ($R\alpha,\gamma$) is then calculated as:

$$R\alpha,\gamma = \mu - \kappa\,\sigma$$

where α = Confidence level

γ = Non-exceedance probability (NEP)

κ = Tolerance factor for normal distribution; depends on α,γ and the sample size

Using the values in Table 2-1, a tolerance limit ($R\alpha,\gamma$) with an 84% NEP and 90% confidence level is determined to be 1.53. Thus an 84% NEP response with a 90% confidence level can be calculated using a scale factor of 0.65 (reciprocal of 1.53) applied to the absolute sum response. A comparison of FSTF responses calculated using the Monticello methodology with the maximum measured FSTF responses in various tests is provided in PUAR Table 1-4.1-4. A copy of this table is attached. The comparison provides an assessment of the conservatism which results when applying the Monticello methodology. The values for maximum measured FSTF response listed in PUAR Table 1-4.1-4 were obtained using the same methods as for NEDE-24840. The FSTF letter report MI-LR-81-01 may have used preliminary test results, or slightly different data reduction or analysis techniques. The differences are very slight between the PUAR and MI-LR-81-01, and do not

affect the conclusions of the comparison of the analysis to the data. The analysis techniques used in the Monticello PUA are conservative and result in predictions that bound the maximum measured FSTF response by a wide margin.

Measured pressure amplitudes from FSTF test M12 were used in the Monticello PUA as a fourth alternate in calculating the response due to the condensation oscillation load. It has been observed that FSTF test M12 condensation oscillation torus shell pressures at certain frequencies are higher than the pressures for the three alternates specified in the LDR. A comparison of the torus responses due to the application of FSTF test M12 amplitudes and amplitudes for the three LDR alternates is shown in Table 2-2. Although this comparison is based on the response of the Fermi 2 torus, similar results are predicted for Monticello since the geometry and the dominant structural frequency of the two plants are similar. The comparison shows that the additional conservatism in the response due to M12 is location dependent and may be as much as 27% greater than that due to the LDR alternates. It is estimated that the fourth alternate (M12) has added about 10% to 30% of additional conservatism to the Monticello CO response.

Table 2-1

TORUS RESPONSE RATIOS FROM

TABLES 6-1 THROUGH 6-3 OF NEDE-24840

RESPONSE QUANTITY	RESPONSE RATIO (Abs. sum / 84% NEP)
1	1.53
2	1.55
3	1.69
4	1.70
5	1.72
6	1.74
7	1.78
8	1.80
9	1.86
10	1.88
11	1.94
12	2.01
13	2.01
14	2.02
Mean (π) value	1.80
Standard Deviation (σ)	0.16

Table 1-4.1-4

FSTF RESPONSE TO CONDENSATION OSCILLATION

RESPONSE QUANTITY	CALCULATED FSTF RESPONSE AT 84% NEP(1)	MAXIMUM MEASURED FSTF RESPONSE		
		M8	M11B	M12
BOTTOM DEAD CENTER AXIAL STRESS (ksi)	3.0	2.3	1.6	2.7
BOTTOM DEAD CENTER HOOP STRESS (ksi)	3.7	2.6	1.4	2.9
BOTTOM DEAD CENTER DISPLACEMENT (in.)	0.17	0.11	0.08	0.14
INSIDE COLUMN FORCE (kips)	184	93	68	109
OUTSIDE COLUMN FORCE (kips)	208	110	81	141

(1) USING CO LOAD ALTERNATES 1, 2, AND 3.

Table 2-2

COMPARISON OF FERMI-2 TORUS RESPONSE DUE TO CONDENSATION OSCILLATION LOAD ALTERNATE 4 (M12) AND THE THREE LDR ALTERNATES

RESPONSE QUANTITY	MAXIMUM RESPONSE		CONSERVATISM DUE TO ALTERNATE 4 (%)
	Alternate 4 (M12)	Alternates 1,2, and 3 from LDR	
Inside Column downward Force (kips)	206.76	182.58	13.2
Outside Column downward Force (kips)	225.44	200.31	12.5
Inside Saddle downward Force (kips)	289.48	261.38	10.8
Outside Saddle downward Force (kips)	350.23	309.98	13.0
Memb. Stress Intensity at Bottom Dead Center near midbay (ksi)	6.57	5.81	13.1
Memb. Stress Intensity at about 60° below equator at miter on outside	8.8	7.81	12.7
Memb. Stress Intensity at 30° above equator near miter	6.44	5.07	27.0

Question 3

The downcomer dynamic load methodology derived from the supplemental FSTF tests was for tied downcomers. Justify the use of the methodology for the untied downcomers as shown in the PUAR.

Response to Question 3

Because Monticello has tied downcomers, this question does not apply to Monticello.

Question 4

The acceptance criteria specified that for multiple downcomer chugging the force per downcomer shall be based on an exceedance probability of 10^{-4} per LOCA. A correlation between load magnitude and probability level derived from a statistical analysis of FSTF data was utilized in the PUA. Provide the details of the correlation and justification for the use of the correlation.

Revised Response to Question 4

The methodology used to compute the probabilities of exceedance for the Monticello multiple downcomer chugging loads shown in PUAR Table 3-2.2-16 is based upon the understanding that the chugging duration of 512 seconds and the number of downcomer chugs of 313 were obtained from FSTF test results.

Further study of the FSTF chugging data report (General Electric Report NEDE-24539-P dated April 1979) indicated that a chugging duration of 512 seconds represents a realistic duration for an actual plant. By dividing the chugging duration of 512 seconds by a conservative chugging period of approximately 1.63 seconds observed in FSTF, a total number of 313 chugs was obtained. It was also observed that not all of the 313 chugs were synchronized pool chugs.

From FSTF Test M1, which is representative of Monticello plant conditions, it was observed that about 33 percent of all the chugs were synchronized pool chugs. The rest of the chugs were not well-synchronized pool chugs and would not result in any multiple downcomer lateral load having the force in the same direction occuring at the same time. Therefore, based upon FSTF Test M1, out of 313 chugs, only about 104 chugs (33 percent) were synchronized pool chugs resulting in a number of downcomers having the lateral force in the same direction at the same time.

Scaling the above information for the conservative chugging duration of 900 seconds, the number of synchronized pool chugs for Monticello will be about 182. In accordance with NUREG-0661, the probability of exceedance for calculating the force per downcomer in multiple downcomer chugging is based on the premise that the force per downcomer would exceed the design load once per LOCA. Thus, for Monticello the probability that the force per downcomer in a pool chug can be exceeded once per LOCA will be the reciprocal of 182 or 5.5×10^{-3}. This probability level is applicable for any number of downcomers considered to be loaded with the same force in the same direction at the same time.

Based upon the above probability of exceedance, the chugging forces per downcomer presented in PUAR Table 3-2.2-16 are bounding for different number of downcomers considered to have the lateral force in the same direction occuring at the same time.

Question 5

(a) On page 1-4.113, it is stated that the peak positive bubble pressure and maximum bubble pressure differential from the Monticello T-quencher test data are 9.9 psid and 18.1 psid, respectively. Table 3-3, Page 3-10, NEDE-21878-P indicates that these values are 9.3 psid and 17.4 psid. Provide information to permit clarification of this discrepancy.

(b) Additional information is required to determine whether modification of the bubble pressure bounding factor from the LDR value of 2.5 to the proposed value of 1.75 is justified. Specifically, the peak positive and negative bubble pressure predicted by the SRV bubble pressure methodology when the 1.75 multiplier is employed should be reported. The initial conditions for this calculation are to correspond to the CP, NWL, SVA case as listed in Table 3-2 of NEDE-21878-P.

Response to Question 5

(a) The peak positive bubble pressure and maximum bubble pressure differential from the Monticello test data are 9.3 psid and 17.4 psid, respectively. The statement in the PUAR regarding the values of 9.9 psid and 18.1 psid

refers to the calculated values of peak positive and maximum bubble pressure differential using the bubble pressure bounding factor of 1.75.

(b) A value of 1.75 produces results which bound peak positive bubble pressure differential from the Monticello T-quencher test data. The calculated values using 1.75 are 9.9 psid and 18.1 psid, respectively. The predicted values correspond to a single valve actuation, normal water level of the cold pop case listed in Table 3-2 of NEDE-21878-P.

This response was incorporated into Section 1-4.2.4 (page 1-4.105 of Revision 1 to the PUAR).

Question 6

The post-chug submerged structure loads, as specified in the acceptance criteria, were to be computed on the basis of the two nearest downcomers chugging at the maximum source strength with phasing between the downcomers that maximizes the local acceleration. On PUAR page 2-2.41 it is stated that the loads were developed using the average source strength. Please clarify the situation by documenting the calculation in detail for the ring girder, giving the source strengths used and their locations.

Response to Question 6

The Monticello PUAR, Revision 1, correctly states that the post-chug submerged structure loads for Monticello were developed using the maximum source strength.

Question 7

Provide a more detailed discussion of the method used to account for FSI effects on condensation oscillation and chugging submerged structure loads. Include an explanation of how the local pool fluid accelerations are determined.

Response to Question 7

A detailed discussion of the method used to account for FSI effects on condensation oscillation and chugging submerged structure loads is provided in the Continuum Dynamics, Inc. Tech Note No. 81-6, Revision 0, "Mark I Methodology for FSI Induced Submerged Structure Fluid Acceleration Drag Loads."

Question 8

Provide a complete description of the bases for the local-to-bulk pool temperature differences which are presented in Section 1-5.1 of the PUAR. The AC (Section 2.13.8.2) stipulates that this parameter should be supported either by existing Monticello pool temperature data or in-plant tests. If the first of these options is employed, the applicant must demonstrate the applicability of the Monticello data base by providing a detailed comparison of the respective quencher and suppression pool geometries. Also, since credit for RHR effectiveness in reducing the local-to-bulk temperature difference is being taken by the applicant, comparison of the suction and discharge geometries of the respective RHR systems should also be provided. If the Monticello data base is used in conjunction with an analytical model to estimate plant unique values of local-to-bulk temperature differences, a complete description of the analyses should be supplied together with a demonstration of the credibility of the model in terms of its ability to accurately predict experimental suppression pool temperature responses to extended SRV discharges.

Response to Question 8

GE analyzed seven postulated long-term SRV events in the Monticello plant to demonstrate conformance with the local pool

temperature limit as defined by the NRC (cf, Reference 16 of the Monticello PUAR). The assumptions and results of this analysis are presented in Section 1-5.1 of the PUAR.

The analysis is based on properly modeling each of the seven events using two GE proprietary computer program to evaluate local and bulk pool temperatures as a function of time.

The first program is a coupled RPV and suppression pool thermodynamics model which calculates the transient response of the suppression pool during long-term events which add heat to the pool. This model performs fluid mass and energy balances in the reactor primary system and the suppression pool and calculates the reactor vessel water level, pressure, and the long-term response of the suppression pool bulk temperature. The various modes of operation of all important auxiliary systems, such as the SRV's, main steam isolation valves (MSIV's), Emergency Core Cooling System (ECCS), Residual Heat Removal (RHR) System, and feedwater are modeled. To simulate a specified reactor cooldown rate or depressurization rate, a rate of change of temperature or pressure may be imposed on the reactor vessel. In addition, the model also simulates system set points (automatic and manual), and specified operator actions. Table 1-5.1-1 of the PUAR provides the calculated maximum suppression pool bulk temperatures of each event.

The second computer program is a local pool temperature model which calculates the water temperature in the vicinity of the quencher during SRV discharge events which add heat to the pool. This program was developed under the Mark I Program expressly to model Mark I plants equipped with T-quencher discharge devices. The model is calibrated to the Monticello test results. Pool temperature distributions predicted by the model have been compared with the Monticello T-quencher test results and the Monticello T-quencher thermal mixing test results. Results of the comparison indicate that the model predicts the local quencher temperature during SRV actuation.

Results from the first model, such as the mass and energy added to and removed from the pool during each transient (i.e., RHR and SRV flows) are inputs into the second model along with pool geometry, submerged structures geometry, and initial pool conditions.

The overall local temperature analysis consists of two major, coupled components: a momentum balance to solve for the bulk pool velocity, and a two-dimensional energy model which determines the temperature distribution in the pool by superimposing the circulation of pool water induced by the SRV discharge on the bulk motion of the pool. The energy model is of sufficient generality to accommodate multiple SRV actuations for random patterns of T-quencher discharge at selected points in time.

The energy model is applied locally at uniformly distributed nodes throughout the pool. One axial node is assigned to each half bay for each of eight horizontal layers. Thus, a total of 16 nodes per bay is used to describe the temperature distribution in the pool. Application of the models to these nodes results in a coupled set of algebraic equations which are solved by successive substitution at each time step. A simple iterative scheme is employed to ensure conservation of energy.

The local temperatures of interest in this analysis are calculated by averaging the temperature of the nodes directly above and below the T-quencher in the downstream portion of the bay. The local temperatures tabulated in Table 1-5.1-1 of the PUAR correspond to the bay with the highest temperature throughout each event calculated in this manner.

The remaining portion of this response pertains to the oral request to address the basis of the Monticello local pool temperature limit curve as given in Figure 1-5.1-1 of the PUAR.

The curve is based on NUREG-0661 and NUREG-0783 (References 1 and 16 of the Monticello PUAR, Volume 1) which collectively state:

1. For all plant transients involving SRV operation during which the steam flux through the quencher

perforations exceeds 94 lbm/ft^2-sec, the suppression pool local temperature shall not exceed 200°F.

2. For all plant transients involving SRV operation during which the steam flux through the quencher perforations is less than 42 lbm/ft^2-sec, the suppression pool temperature shall be at least 20°F subcooled.

3. For all plant transients involving SRV operation during which the steam flux through the quencher perforations exceeds 42 lbm/ft^2-sec, but is less than 94 lbm/ft^2-sec, the suppression pool local temperature is obtained by linearly interpolating the local temperatures established previously in Items 1 and 2.

Monticello T-quenchers have a submergence of 6.5 feet of water, corresponding to 17.4 psia. The saturation temperature at 17.4 psia is 220.6°F. Thus, for Limit 2, a 20°F subcooling translates into a suppression pool local temperature limit of 200.6°F.

Since the steam mass flux through the quencher perforations is directly dependent on reactor vessel pressure, mass fluxes of 42 lbm/ft^2-sec and 94 lbm/ft^2-sec correspond to reactor vessel pressures of 202 psia and 457 psia, respectively.

The maximum local pool temperature of 194°F calculated for Case 2A (rapid depressurization at isolated hot shutdown assuming one RHR loop available) occurs at a time when the quencher mass fluxes are far below 42 lbm/ft^2-sec, which defines the region where the NRC limit is 200.6°F. Therefore, the maximum local pool temperature for this case lies below the NRC limit. Table 1-5.1-1 of the Monticello PUAR shows the maximum local pool temperatures of all other cases also remained below the NRC limit throughout the transient. Considering the degraded assumptions employed for each case and the conservatism of the NRC limit, the results are considered acceptable, and unstable steam condensation would not be expected.

Question 9

The description of the Suppression Pool Temperature Monitoring System (SPTMS) which is provided in the PUAR is inadequate. Additional information is needed to provide a clear demonstration that the Monticello SPTMS design is in accordance with the requirements of AC Section 2.13.8.3.

Response to Question 9

The Suppression Pool Temperature Monitoring System (SPTMS) for the Monticello Nuclear Generating Plant is an integral part of the overall post-accident monitoring capability of the plant. The SPTMS consists of two independent and redundant safety-related divisions. The safety function of the SPTMS is to provide the plant operator with reliable information on the suppression pool temperature such that the plant can be operated within Technical Specification limits. All components for the system are classified as Class 1E, Seismic Category I, Quality Group B, and the system is designed in accordance with the applicable portions of NUREG-0661 and Regulatory Guide 1.97, Revision 2. All SPTMS safety-related equipment was purchased qualified to the requirements of IEEE Standards 323-1974 and 344-1975. Each division of the SPTMS is physically separated from the other, and either division is capable of providing an accurate measure of the suppression pool bulk temperature.

Each division of the SPTMS has eight thermowells (one redundant pair) located in each of the discharging bays of the suppression chamber. The thermowells are located approximately symmetrical around the outside of the suppression chamber at the centroid elevation of the suppression pool water mass. The centroid elevation is much below the suppression pool drawdown level, so that uncovering of the thermowells after a LOCA will not occur. The redundant thermowells of each division in each discharging bay are located approximately six feet apart. The locations of the thermowells on the suppression chamber wall were chosen so that the response of the thermowells would lead the actual bulk temperature and give a conservative answer. A simple averaging algorithm is utilized to determine bulk temperature, and each division measures and calculates bulk temperature.

Bulk pool temperature is utilized since the plant's technical specifications are based on bulk temperatures. Resistance temperature detectors (RTD's) are used within each thermowell to measure the temperature. Each division has a microprocessor which takes the data from each of the eight RTD's within that division and calculates a bulk pool temperature. The microprocessor also has a strip chart recorder which records individual RTD temperatures and the bulk pool temperature. Each division also has a remote control unit in the control room. The

remote control unit has the capability to display individual RTD temperatures, the bulk pool temperature, and alarm at the Technical Specification limits. The remote control unit will also alarm if it detects a failure of one of the RTD's. The microprocessor unit sends a signal to the process computer and is equipped to provide a signal to the Safety Parameter Display System as needed. Printouts of the temperature at the individual temperature sensors, the bulk temperature, calendar date, and time of day are available under the following conditions:

- On demand by punching a button on the keypad.
- Every hour on the hour when the bulk temperature is less than 90°F.
- Every minute when the bulk temperature is greater than or equal to 90°F and is less than or equal to 120°F.
- Every five minutes when the bulk temperature is greater than 120°F.

The operability of the system will be checked by utilizing automatic self-testing of the following areas:

- The validity of the temperature sensor inputs
- The capability of the processor to perform data acquisition, calculation, and communication functions
- The validity of the alarm relay contact settings.

Figures 1 and 2 show the system configuration and the thermowell/RTD locations.

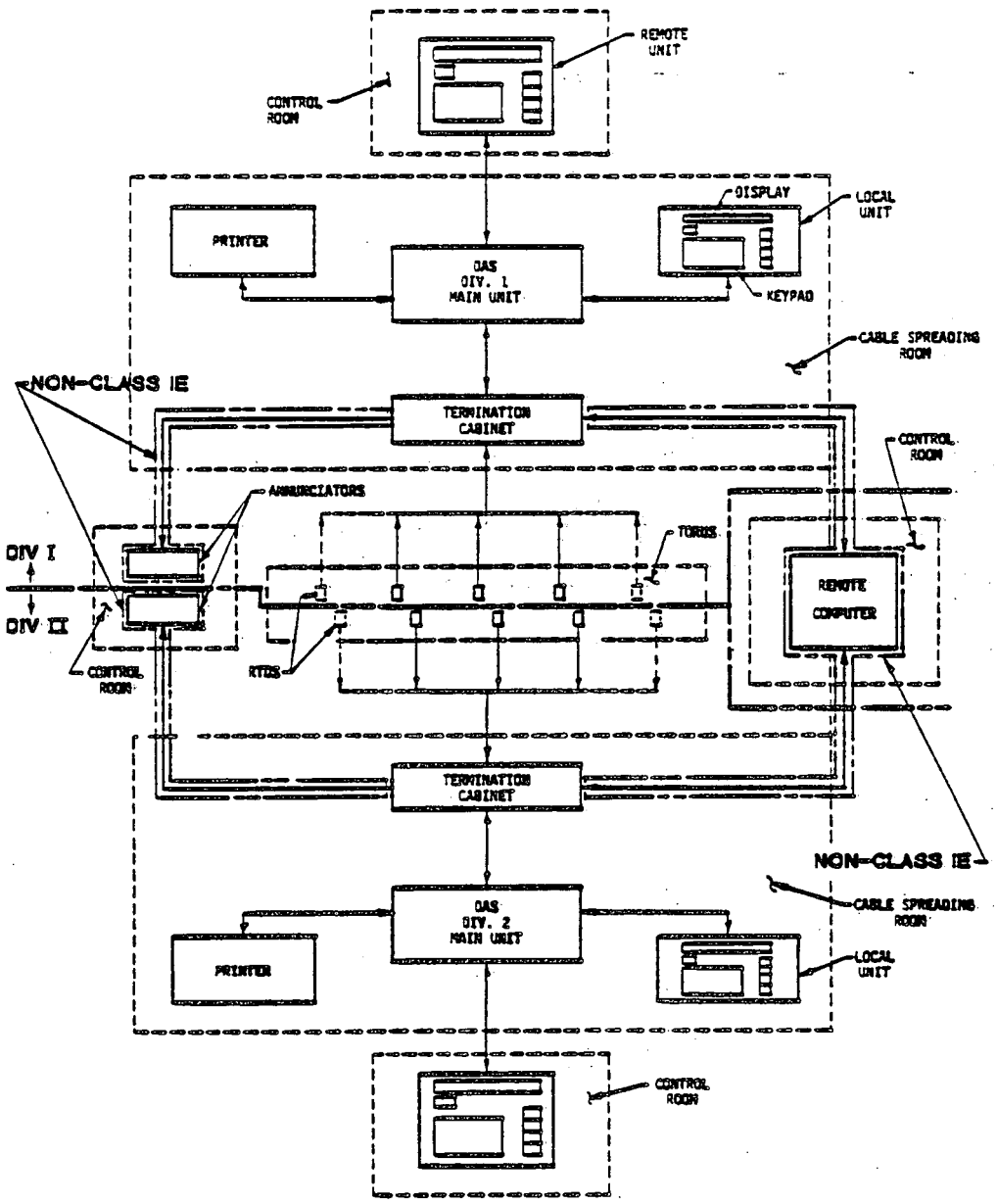

Figure 1

SYSTEM ARCHITECTURE

nutech ENGINEERS

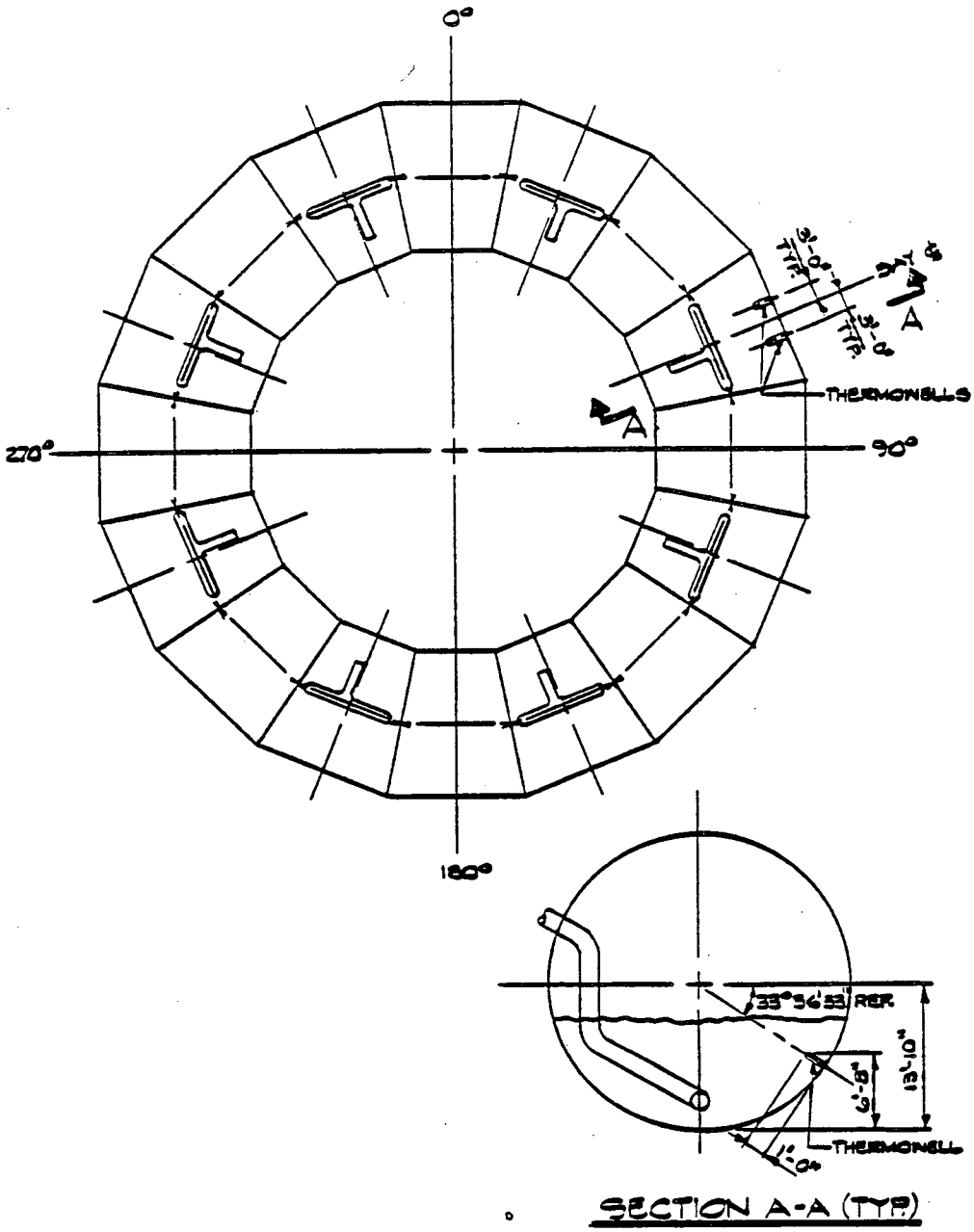

Figure 2

RTD ASSEMBLY LOCATIONS

nutech ENGINEERS

Question 10.1

With regard to suppression chamber analysis, provide justification for not analyzing a 180° beam segment including the torus, columns, and seismic restraints as required by the criteria for considering the effect of seismic and other lateral loads. Also, discuss the implications of this approach with regard to stresses in the suppression chamber in the region surrounding the support columns.

Response to Question 10.1

The approach used in the Monticello PUAR to evaluate suppression chamber lateral loads results in loads which compare to those obtained from a 180° beam model. As discussed in PUAR Section 2-2.4.2, accelerations and dynamic load factors based on the suppression chamber lateral frequency, taken from the FSAR, are used to develop lateral loads for seismic loads and for asymmetric torus shell loads due to SRV discharge and pre-chug. The resulting lateral loads are added absolutely to obtain a bounding value of the total suppression chamber lateral load, which is conservatively assumed to be transferred by two of the four seismic restraints.

The total lateral load which would be produced by a 180° beam model would also be based on the response to each loading at the

dominant lateral frequency of the suppression chamber. However, a 180° model analysis would result in more support column participation and less load at the seismic restraint. This approach would also result in less stress in the suppression chamber shell adjacent to the seismic restraint than that determined in the Monticello PUA.

Lateral loads result in a shear effect and an overturning moment effect on the suppression chamber. The horizontal shear effect is the more significant component and is resisted by the seismic restraints shown in Figure 2-2.1-12. The overturning moment effect results in vertical loads which are resisted at each miter joint by the suppression chamber columns and miter joint saddles shown in Figure 2-2.1-3. The vertical loads on any one column/saddle assembly are small compared with those caused by the major torus shell loadings which primarily act in the vertical direction, the results of which are shown in Tables 2-2.5-7 and 2-2.5-8. The corresponding stresses in the suppression chamber shell adjacent to the column/saddle assembly due to the overturning moment would also be small.

Question 10.2

With regard to the assumption that only 20% of the total mass of water in the suppression chamber contributes to lateral seismic loads, provide justification to indicate the applicability of the tests cited in the PUA report to support this assumption.

Response to Question 10.2

For a suppression chamber partially filled with water subjected to a horizontal seismic excitation, a portion of the total water mass acts as a rigidly attached mass while the remaining water mass acts in sloshing modes. The effective weight of water which acts as a rigidly attached mass was determined from 1/30 scale generic tests performed as part of the Mark I program effort. The seismic slosh test facility is identical and the test procedures used to determine the effective water weight are similar to the tests described in General Electric Report NEDC-23702-P, "Mark I Containment Program Seismic Slosh Evaluation," March 1978.

The 1/30 scale model test facility is based on a prototypical Mark I suppression chamber whose geometric characteristics are very close to those of Monticello. Tests were performed with three different support stiffnesses (rigid, medium, and flexible), which covered the range of stiffnesses and frequencies for

all Mark I plants, including Monticello. The analytical model developed for use in the referenced study predicts that 20% of the total mass of water acts as a rigidly attached mass with the suppression chamber. This prediction was verified with the 1/30 scale model by comparing the measured frequencies of the test facility with those obtained from the analytical model. This was done by first adjusting the emptied test facility support stiffness to that necessary to obtain the frequency of the empty suppression chamber predicted by the analytical model. The test facility was subsequently filled with water to a height below the equator, and a series of tests were performed to determine the frequency. The resulting frequencies compared favorably with those obtained using the analytical model with the same assumed water height. The test results therefore confirm the analytical results which showed that 20% of the total water mass acts as a rigidly attached mass. These results are considered applicable for use in evaluating the Monticello suppression chamber response to seismic loadings.

The evaluation of the Monticello suppression chamber for horizontal seismic loads is discussed in Section 2-2.4.2 of the PUAR. The seismic lateral load is calculated assuming that 20% of the total water mass acts at a spectral acceleration of 0.07g. The remaining 80% of water is assumed to act at the maximum accelerations in the range of sloshing frequencies. The methodology accounts for 100% of the water and results in a bounding value for the suppression chamber lateral load due to seismic loads.

Question 10.3a

Provide detailed calculations to indicate how the modal correction factors given in Sections 1-4.2.3 and 2-2.4.1 of the PUA report are obtained.

Response to Question 10.3a

Modal correction factors used in calculating the response due to SRV torus shell loads are obtained by dividing the response of an initial value or free vibration problem by that of a transient forced vibration response problem. The physical representations for the analogs used in developing these correction factors are shown in Figure 10.3-1. Two representations of source pressure in a rigid tank are shown. The transient response problem consists of a rigid torus with a pressure source, P_B, which is prescribed as a decaying cosine function. The initial value problem consists of a similar torus which contains a spring and disk mechanism for providing an impulse to the surrounding pool water.

The analogs, described in terms of masses and springs, are shown in Figure 10.3-2 for the transient response or forced vibration problem and the initial value or free vibration problem. The torus system is described in terms of a generalized stiffness, k_s, and a generalized mass, m_s.

The forced vibration analog is subjected to an applied loading, described as

$$P_B(t) = P_B e^{-\lambda t} \cos \omega_B t$$

where,

P_B = bubble force at time equal to zero

λ = attenuation constant

ω_B = frequency of the SRV bubble

t = time

The free vibration analog incorporates an additional mass and spring, representing the bubble system, which is utilized to establish a frequency of the bubble oscillation. The apparent or effective mass of the bubble is defined as m_B. The numerical value of an apparent bubble mass is estimated by averaging the hydrodynamic mass for the case of an oscillating sphere in a still fluid and a fixed sphere in an oscillating fluid. The bubble stiffness is computed by multiplying the bubble mass by the bubble frequency squared.

Four spherical bubbles are assumed for the T-quencher discharge device. Single bubble stiffnesses are additive since the bubbles are assumed to act in phase (i.e., parallel springs).

The initial conditions for the free vibration analog are prescribed by compressing the spring, k_B, a distance, $\Delta\ell$, such

that at time equal to zero the force in the spring is equal to P_B. Therefore, at time equal to zero, both the forced vibration and free vibration analog have the same applied load magnitude.

Damping for the torus system can be described in terms of load attenuation and structural damping. Based upon test observations, it is assumed that the structural response will be decayed in the same manner as the prescribed pressure. Accordingly, a decaying exponential function of the form $e^{-\lambda t}$ is used to represent load attenuation and structural damping in the solution of the forced and free vibration system, respectively.

The equations of motion for the free vibration analog described in Figure 10.3-2 are obtained from free body diagrams for the structure mass and bubble mass as

$$m_s \ddot{X}_s - (k_s + k_B) X_s + k_B X_B = 0$$

$$m_B \ddot{X}_B - k_B X_B + k_B X_s = 0$$

where,

X_s = structure mass displacement

$\ddot{X}_s$ = structure mass acceleration

X_B = bubble mass displacement

$\ddot{X}_B$ = bubble mass acceleration

The solution to these equations expressed in terms of the structure response, X_s, is given as the following function,

$$X_s = \frac{P_B}{k_s} e^{-\lambda t} f_1\left(\frac{\omega_B}{\omega_s}, \frac{k_B}{k_s}, \frac{k_B}{m_s}\right)$$

where,

ω_B = bubble frequency

ω_s = structure frequency

The other variables have been previously defined.

A family of curves which represents dynamic load factors as a function of frequency (ω_B/ω_s) is generated by assuming either (k_B/m_s) or (m_B/m_s) as constant. Based upon estimates of the significant modal characteristics of the torus and the oscillating bubble, a range of values for (k_B/m_s) and (m_B/m_s) is established. The range of (k_B/m_s) values is estimated to be about 160 to 1600. The range of (m_B/m_s) values is estimated to be 0.03 to 0.3.

Figure 10.3-3 contains a comparison of DLF's for the cases with (k_B/m_s) equal to 160 and 1600, assuming a structural frequency of 20 Hz. The maximum DLF for the case with (k_B/m_s) equal to 160 is 2.8, whereas for (k_B/m_s) equal to 1600, the maximum DLF is 2.0. It was determined that the DLF's for the case with (k_B/m_s) equal to a constant are about 20 to 60 percent larger than the DLF's for the case with (m_B/m_s) equal to a constant.

The equation of motion for the forced vibration analog described in Figure 10.3-2 is obtained from the free body diagram for the structure mass as:

$$m_s X_s - k_s X_s = P_B e^{-\lambda t} \cos \omega_B t$$

The solution to this equation is given in the following function:

$$X_s = \frac{P_B}{k_s} e^{-\lambda t} f_2(\omega_B, \omega_s, \lambda)$$

Figure 10.3-4 contains DLF's plotted as a function of (ω_B/ω_s). A family of DLF curves is included for structure frequencies of 11, 14, and 20 Hz. The DLF's for the resonant condition range from 5.4 to 9.9 for structural frequencies between 11 and 20 Hz. The forced vibration DLF's are approximately 3 to 5 times the free vibration DLF's.

Correction factors are obtained by dividing the free vibration response to the system by the response of the forced vibration system. The sensitivity of the correction factor to the variables $(k_b/m_s, m_B/m_s, \lambda)$ is evaluated in order to determine a valid set of correction factor curves to be used in design.

Based upon the above evaluation, it was determined that the lower range of (k_B/m_s) should be used for determining conservative design basis modal correction factors. An attenuation factor of

6 is selected, since use of this factor results in correction factors which bound the response at resonance conditions for all structural frequencies.

A typical correction factor curve is shown in Figure 10.3-5 for a structural frequency of 20 Hz. For the plant unique analysis, a set of enveloping correction factors is generated for different modal frequencies of interest, as shown in PUAR Figure 2-2.4-10.

Table 10.3-1 contains a comparison of analytical results obtained using modal correction factors and measured results for Monticello. The results shown are obtained by dividing analytical results by test results for key response parameters. The comparisons show that modal correction factors provide a conservative basis for calibrating the analytical model used to evaluate the response of the Monticello suppression chamber for SRV torus shell loads. The modal correction factors are developed at test conditions and applied at design conditions in accordance with NUREG-0661.

Table 10.3-1

CORRECTED TRANSIENT RESPONSE ANALYSIS

NORMALIZED BY TEST RESPONSE

LOCATION	COMPONENT	TEST CONDITION	
		COLD POP	HOT POP
	a) Stress Intensity		
78° From Inside Equator Midbay	Shell Membrane	1.2	1.3
78° From Outside Equator Midbay	Shell Membrane	1.4	2.3
	b) Column Reaction		
Inside Support Column	Upload	3.7	3.0
Inside Support Column	Download	2.8	2.0
Outside Support Column	Upload	4.4	3.5
Outside Support Column	Download	2.7	2.8

$$P_B(t) = P_B e^{-\lambda t} \cos \omega_B t$$

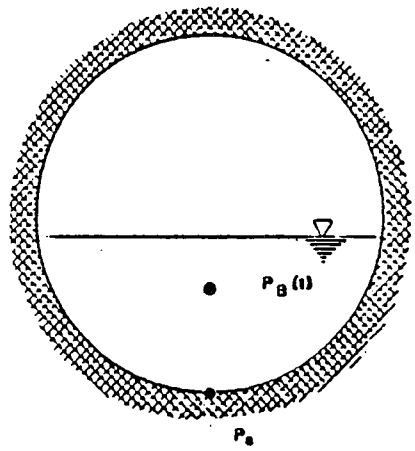

a) TRANSIENT DEFINITION

AT TIME ZERO: $P_B = \frac{k_B \Delta l}{A}$

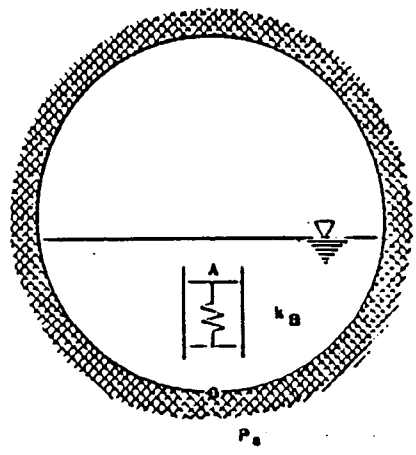

b) INITIAL VALUE DEFINITION

Figure 10.3-1

SRV LOAD DEFINITION

nutech ENGINEERS

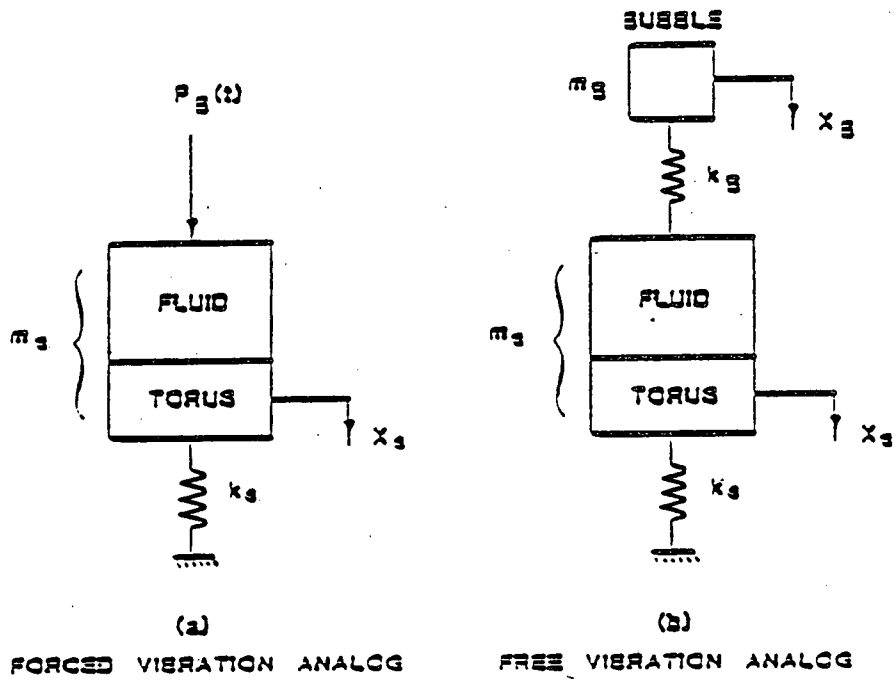

Figure 10.3-2

STRUCTURAL RESPONSE ANALOGS

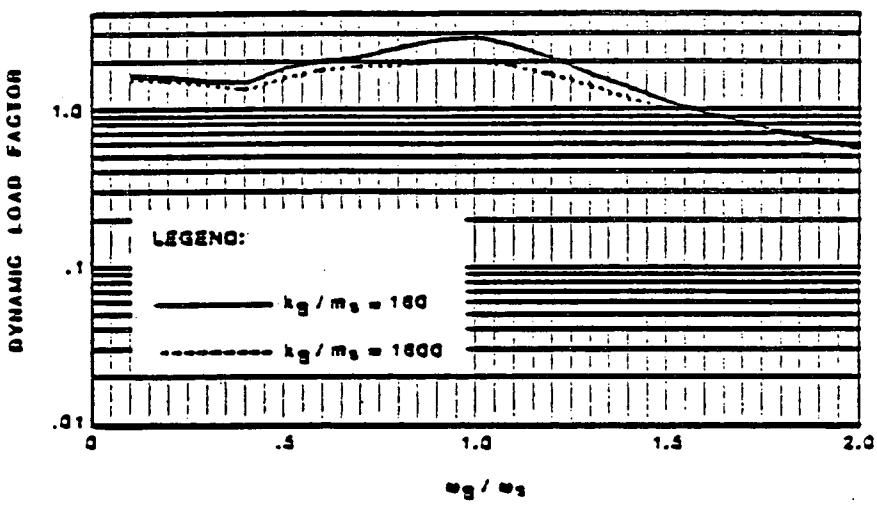

Figure 10.3-3

FREE VIBRATION ANALOG DYNAMIC LOAD FACTORS FOR (k_B/m_s) CONSTANT

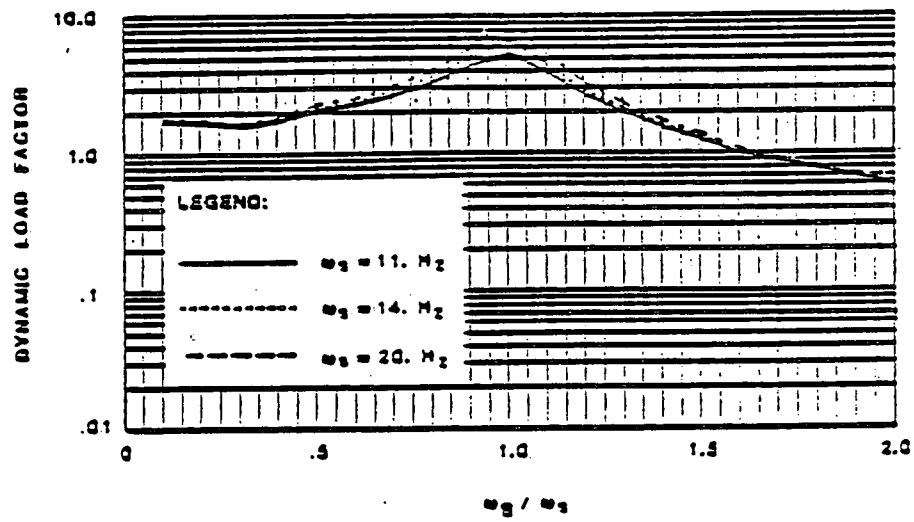

Figure 10.3-4

FORCED VIBRATION ANALOG DYNAMIC LOAD FACTORS

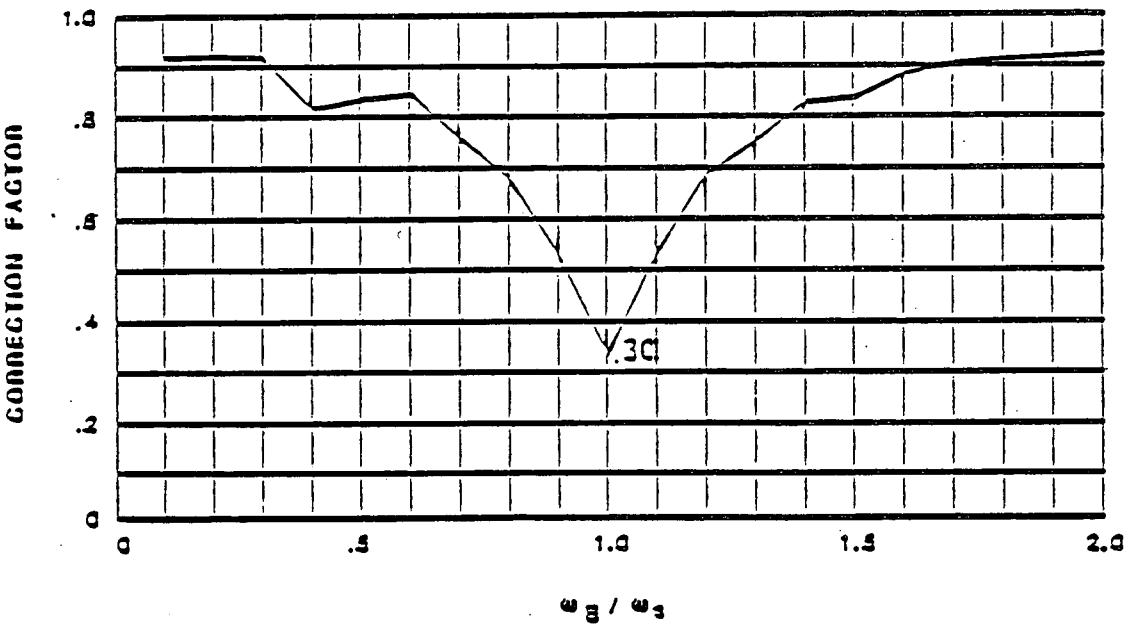

Figure 10.3-5

TYPICAL MODAL CORRECTION FACTOR

Question 10.3b

Provide justification for the applicability of these factors to "multidegree of freedom" systems since the factors were developed using simple "one degree of freedom" systems.

Response to Question 10.3b

The transient response of the Monticello suppression chamber due to SRV torus shell loads is obtained using the modal superposition method. Using this approach, the equations of motion for a multi-degree of freedom system, such as the suppression chamber, are decoupled into a set of equivalent single degree of freedom systems. Each structural frequency or mode is represented by a single degree of freedom system. The responses of each single degree of freedom system are summed to obtain the total response of the suppression chamber.

During the summation process, modal correction factors obtained from PUAR Figure 2-2.4-10 are applied to the response of each single degree of freedom system for each suppression chamber frequency. As discussed in the response to Question 10.3a, the modal correction factors are developed using single degree of freedom systems and are compatible for use in the modal superposition method since this method is completely linear.

Question 10.4

Provide justification for not considering the effect of bending moments in column analysis using interaction formulae.

Response to Question 10.4

The allowable loads for the suppression chamber support columns are shown in Table 2-2.3-2 of the PUAR. These allowables are based on an evaluation of the column-to-shell connection and the column pin and clevis plate assembly, as well as the effect of bending on the columns themselves using the interaction formulae. This evaluation indicates that the allowable column load is controlled by the stress at the column-to-shell connection.

The support column properties and allowables used in Equations 19 and 20 of Appendix XVII of the ASME Code (interaction formulae), are shown in Table 10.4-1. Note that the yield stresses are based on mill tests. The resulting interaction diagrams are shown in Figures 10.4-1 through 10.4-4. Finally, Table 10.4-2 shows a comparison of allowable moments and calculated moments for the DBA III load combination because this combination results in the maximum compressive load on the columns.

Table 10.4-1

COLUMN PROPERTIES

$$F_a = \frac{\left[1 - \frac{(Kl/r)^2}{2C_c^2}\right]F_y}{\frac{5}{3} + \frac{3(Kl/r)}{8C_c} - \frac{(Kl/r)^3}{8C_c^3}} \qquad \text{where } C_c = \sqrt{\frac{2\pi^2 E}{F_y}} \qquad \text{and } E = 27.9 \times 10^3 \text{ KSI}$$

for F_y = 39.8 ksi, C_c = 117.63
F_y = 43.1 ksi, C_c = 113.04
F_y = 50.5 ksi, C_c = 104.43

$$F_a' = \frac{12\pi^2 E}{23(Kl_b/r_b)^2} \qquad F_{bx} = .66F_y$$

	MATL & F_y		AREA (IN^2)		S_{xx} (IN^3)		r (IN)					KL/r					F_a (KSI)		F'_{ex} (KSI)		F_{bx} (KSI)	
							X-X AXIS		Y-Y AXIS			X-X AXIS		Y-Y AXIS								
COLUMNS	EXISTING COL.	ADDED REIN.	WITHOUT REIN.	WITH REIN.	WITHOUT REIN.	WITH REIN.	WITHOUT REIN.	WITH REIN.	WITHOUT REIN.	WITH REIN.	l (IN)	WITHOUT REIN.	WITH REIN.	WITHOUT REIN.	WITH REIN.	C_{ms}	WITHOUT REIN.	WITH REIN.	WITHOUT REIN.	WITH REIN.	WITHOUT REIN.	WITH REIN.
I.S.	API 5LX-X42 43.1	SA106 GR B 39.8	23.94	51.14	41.0	100.5	2.72	3.25	2.72	3.00	80.25	29.54	24.69	29.54	26.75	0.6	23.62	22.15	164.6	235.7	28.46	26.27
O.S.	API 5LX-X42 50.5	SA106 GR B 39.8	31.30	58.50	49.4	82.1	2.61	2.66	2.61	3.50	104.25	39.99	39.26	39.99	29.75	0.6	25.95	21.03	89.84	93.21	33.33	26.27
[1]	[2]	[3]	[4]	[5]	[6]	[7]	[8]	[9]	[10]	[11]	[12]	[13]	[14]	[15]	[16]	[17]	[18]	[19]	[20]	[21]	[22]	[23]

REINFORCED GEOMETRY

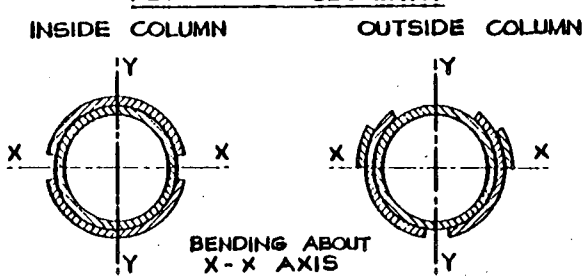

nutech ENGINEERS

Table 10.4-2

COMPARISON OF ALLOWABLE AND CALCULATED MOMENTS FOR LOAD COMBINATION DBA III

LOCATION	AXIAL LOAD	ALLOWABLE MOMENT	CALCULATED MOMENT	CALCULATED ALLOWABLE
INSIDE COLUMN	605.51	1330.6	279.51	0.21
OUTSIDE COLUMN	642.13	1164.65	479.95	0.41

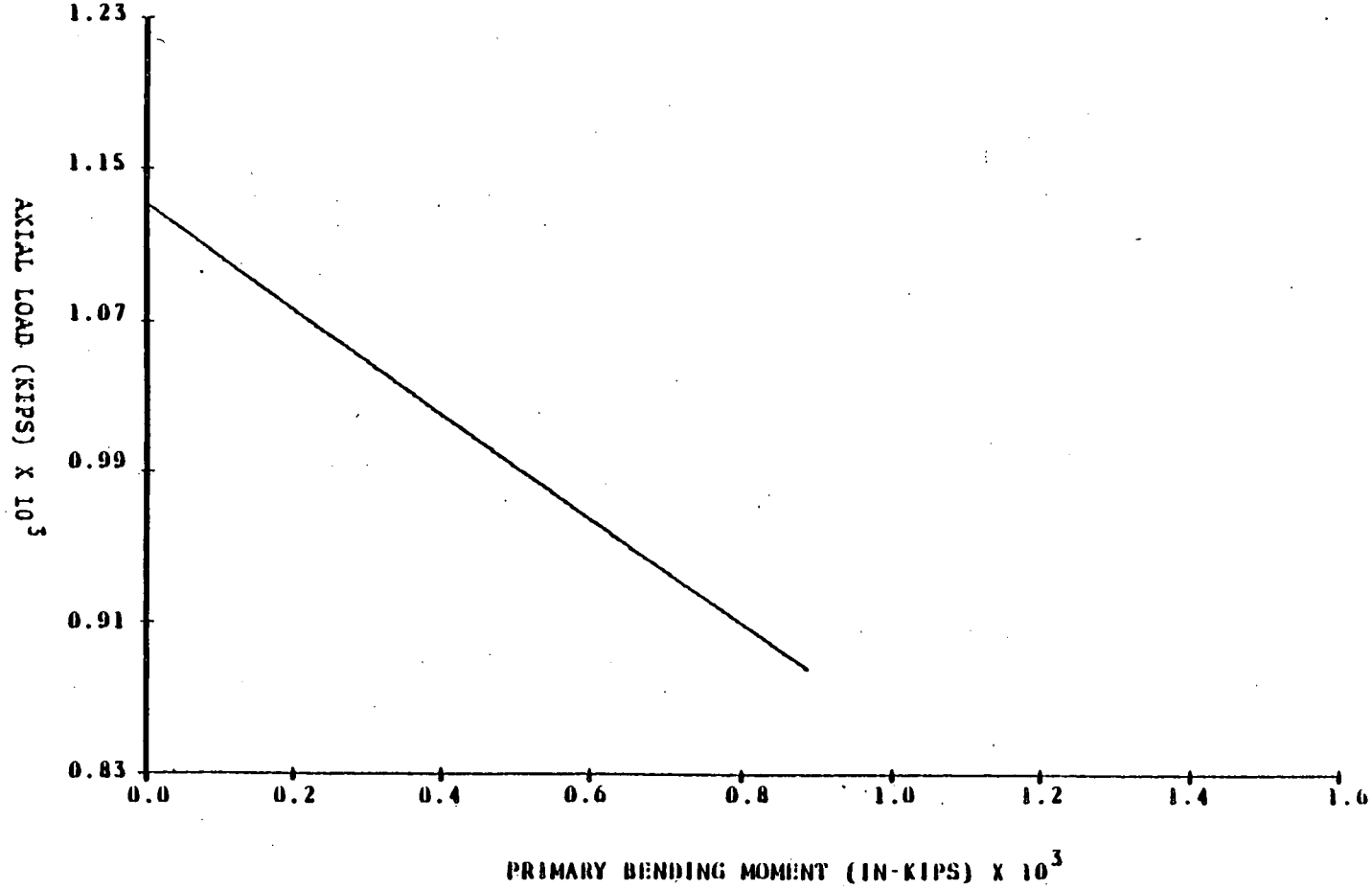

Figure 10.4-1

CODE ALLOWABLE LOAD - MOMENT INTERACTION DIAGRAM
EQ 19 (APPENDIX XVII) EVALUATED FOR PRIMARY STRESSES
MONTICELLO INSIDE COLUMN

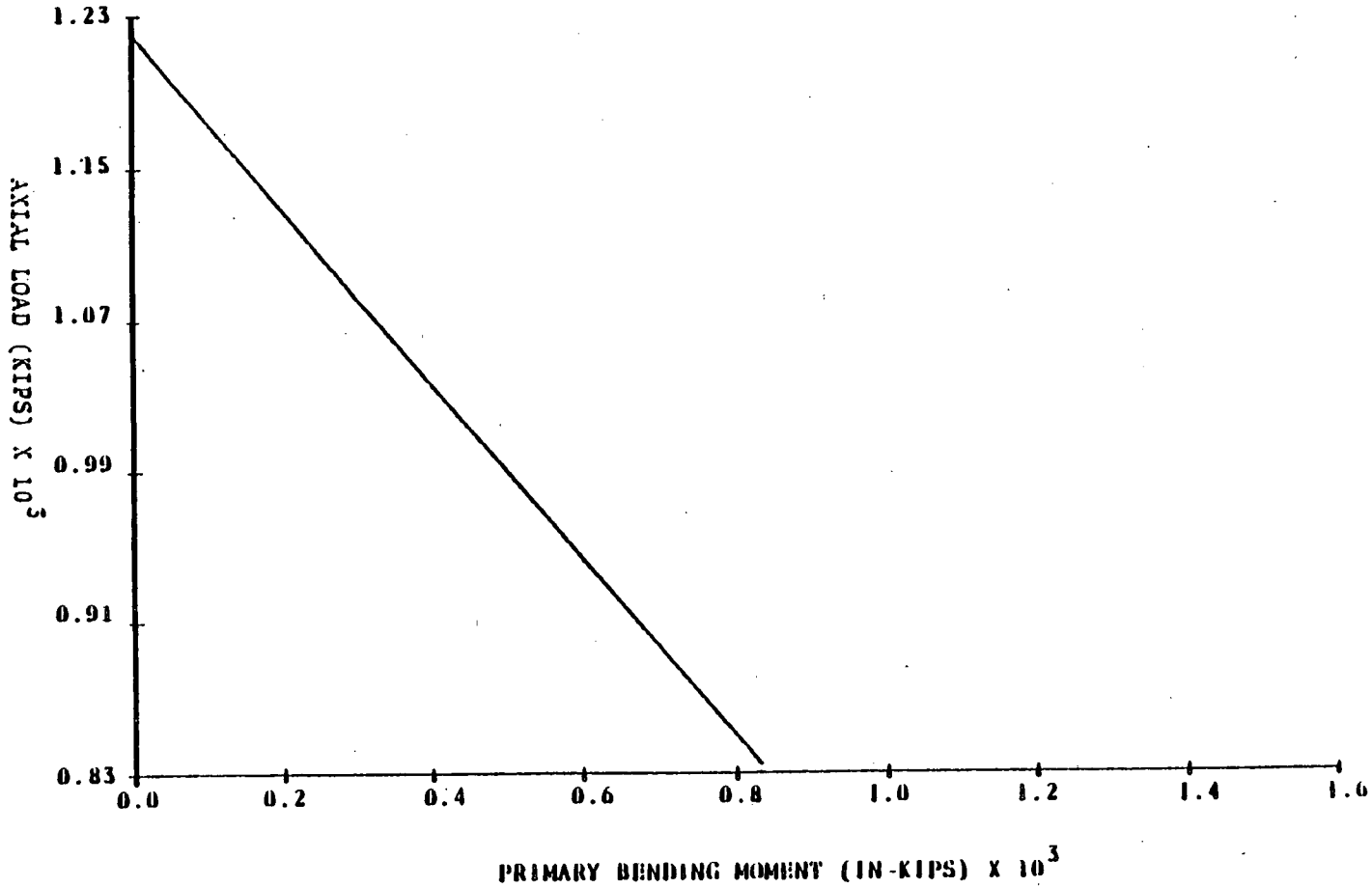

Figure 10.4-2

CODE ALLOWABLE LOAD - MOMENT INTERACTION DIAGRAM
EQ 20 (APPENDIX XVII) EVALUATED FOR PRIMARY STRESSES
MONTICELLO INSIDE COLUMN

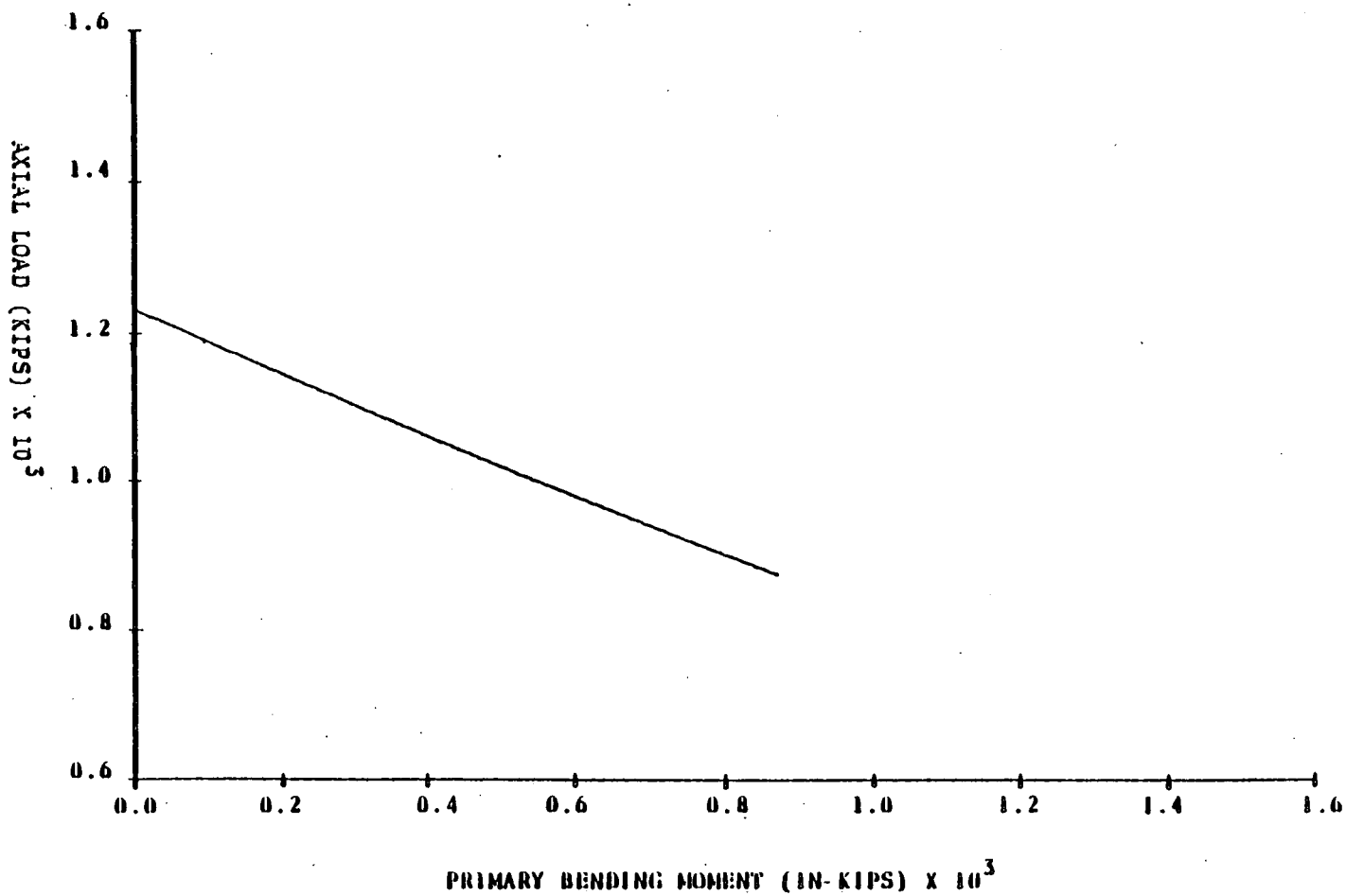

Figure 10.4-3

CODE ALLOWABLE LOAD - MOMENT INTERACTION DIAGRAM
EQ 19 (APPENDIX XVII) EVALUATED FOR PRIMARY STRESSES
MONTICELLO OUTSIDE COLUMN

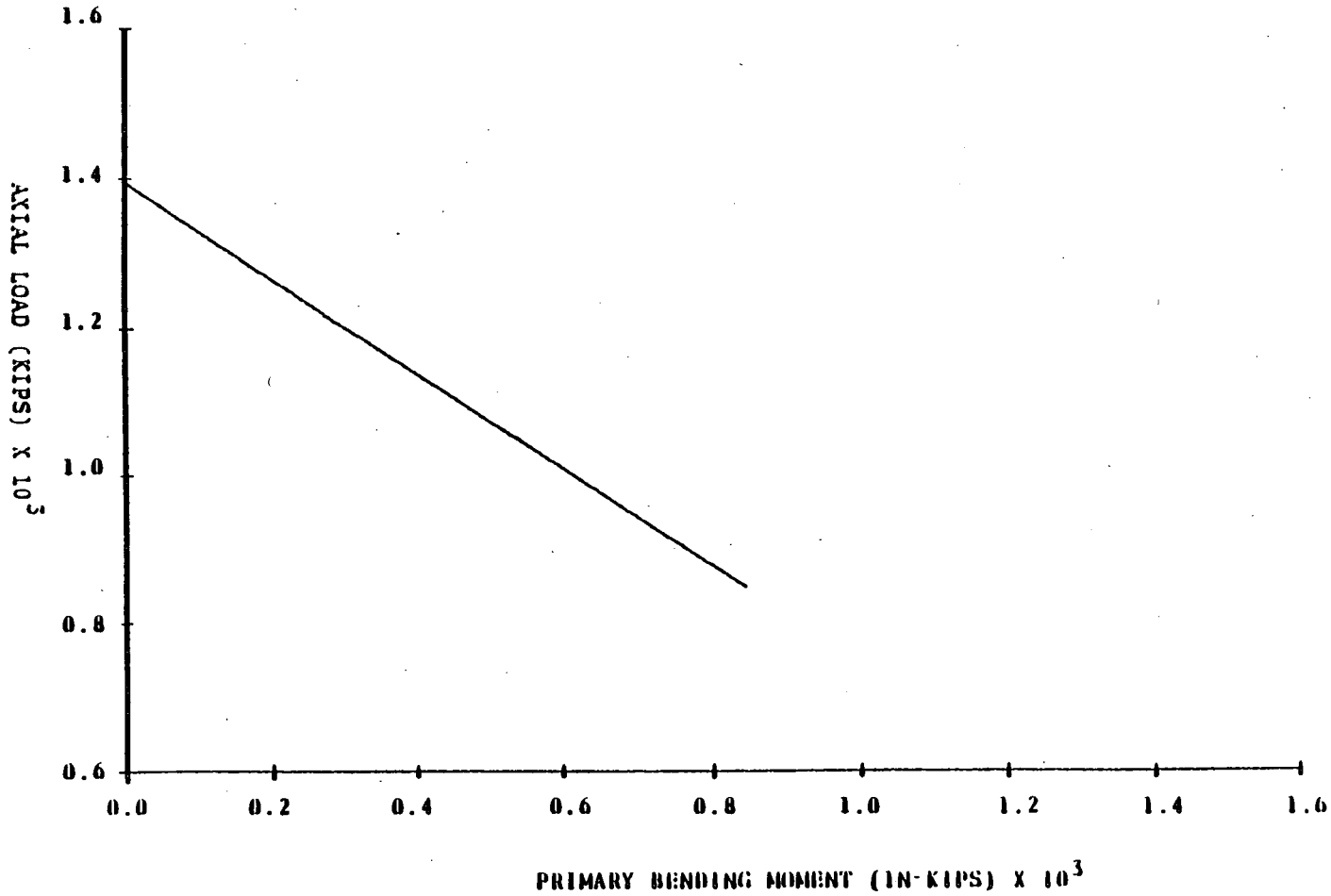

Figure 10.4-4

CODE ALLOWABLE LOAD - MOMENT INTERACTION DIAGRAM
EQ 20 (APPENDIX XVII) EVALUATED FOR PRIMARY STRESSES
MONTICELLO OUTSIDE COLUMN

Question 10.5

With regard to the suppression chamber columns, provide justification and/or additional information to indicate why a nonlinear time history analysis was not performed as required by the criteria when net tensile forces are produced in the columns. Table 2-2.5-2 of the PUA report indicates that net tensile forces are produced in the columns.

Response to Question 10.5

The criteria requirements for performing a nonlinear time history analysis are applicable for plants in which the suppression chamber and its supports are not anchored to the basemat. Such a condition would result in gross nonlinear behavior if uplift loads exceeded the weight of the suppression chamber and contained water.

The Monticello suppression chamber is fully anchored to the basemat at each miter joint column and saddle base plate location, as shown in PUAR Figures 2-2.1-10 and 2-2.1-11. Although tensile forces are produced in the column and saddle supports, the tensile forces are within the allowable anchorage capacity of the support system, as shown in PUAR Tables 2-2.5-7 and 2-2.5-8. The requirements for a nonlinear analysis, therefore, need not be evaluated for Monticello since the

suppression chamber is fully anchored to the basemat and the effects of non-linearities on the overall suppression chamber response have been minimized.

Question 10.6

Provide justification for using two different temperatures, 167°F for suppression chamber and vertical support systems and 100°F for the base plate of the support system, for calculating the respective allowable stresses.

Response to Question 10.6

The allowable stresses for the suppression chamber and its vertical supports are conservatively determined at 167°F since this is the maximum temperature specified for any LOCA event, as shown in PUAR Figures 2-2.2-4 through 2-2.2-6. The allowable stresses for the vertical support system base plates are determined at 100°F, which bounds the maximum temperatures of the base plate expected during the specified events. There may be long-term conditions which result in higher base plate temperatures; however, base plate temperatures higher than 100°F are not expected to occur during times of peak transfer of hydrodynamic loads to the suppression chamber vertical support system. Furthermore, the allowable stresses at 100°F and 167°F are not significantly different.

Question 11.1

Provide justification for using SRSS method to combine the SSE and LOCA responses for SRV piping analysis instead of the absolute sum or cumulative distribution function approaches as required by the criteria.

Response to Question 11.1

The method of combining responses due to LOCA and SSE loads for SRVDL piping described in Section 5-2.2.3 of the plant unique analysis report (PUAR) is based on NRC document NUREG-0484, Revision 1, "Methodology for Combining Dynamic Responses," published in May 1980. The original issue of NUREG-0484 justified combination of responses due to LOCA and SSE within the reactor coolant pressure boundary using the SRSS technique. The current Revision 1 has extended the application of this combination technique to include ASME Code, Section III, Class 1,2, and 3 systems, components, and supports. As described in Revision 1 of NUREG-0484, use of the SRSS technique provides a non-exceedance probability of 84% or higher. Since the Monticello SRVDL piping is analyzed as Class 2 (as prescribed in NUREG-0661), the use of the SRSS method is deemed acceptable based on Revision 1 of NUREG-0484.

Question 11.2

Provide justification for using Markl's equation for fatigue analysis of SRV piping instead of the SN curve given in ASME Code Section III, Division 1 Appendices.

Response to Question 11.2

In order to resolve the issue of piping fatigue, discussions were held between the NRC and the Mark I Owner's Group. These discussions resulted in a commitment by the Mark I utilities to perform a generic fatigue evaluation for SRV piping in the torus and for torus-attached piping systems as part of the plant unique analyses.

Discussions among Mark I Owners and their AE's followed and a taskforce was formed to develop a generic approach for fatigue evaluation. The approach agreed upon was a method which extended the Class 2 piping fatigue rules for thermal fatigue evaluation to include all cyclic loads. A comparison of the extended Class 2 method to a Class 1 fatigue analysis was also provided which showed that the two methods yield similar results.

Elements of the generic approach incorporated are as follows:

- Fatigue usage is evaluated based on consideration of critical loading combinations instead of on an individual load basis.

- Total cumulative fatigue usage for all cyclic loadings is calculated in lieu of monitoring SRV actuations.

- The allowable number of stress cycles is determined by using Markl's equation (Reference 11.2-1) in lieu of the Class 2 thermal fatigue equation basis. (Markl's equation forms the basis for Class 2 piping fatigue and was used in developing the Class 2 piping Stress Intensification Factors).

- Actual stress cycles for a given response time-history are converted into equivalent full stress cycles using the methodology defined in Section NC-3611.2(e)(3) of the Code.

The SRV piping fatigue evaluation performed for Monticello, and documented in Volume 5 of the PUAR, was performed as part of this generic extended Class 2 approach. Utilization of this generic

method results in a more practical, comprehensive method of evaluation for fatigue.

Reference 11.2-1 - Markl, A.R.C., "Fatigue Test of Piping Components," Transactions ASME, Volume 74.

Question 11.3

Provide justification for not using Equation 11 of ASME Code Section III, Subsection NB for calculating the fatigue stresses, and explain the method used.

Response to Question 11.3

Justification for not using Equation 11 of the ASME Code, Section III, Subsection NB (Class 1 Piping) is provided in the response to Question 11.2. Equation 11 of Subsection NC (Class 2 Piping) of the ASME Code provides combination methods for thermal and other sustained loads used in evaluating for fatigue. The methods applied in the Monticello PUAR extended the traditional usage of Equation 11 to allow combination of stresses due to dynamic cyclic loadings, using the same method of absolute summation of stresses.

Question 11.4

Provide justification and reference for the maximum-stress cycle factors given in Table 5-2.4-4 of the PUA report.

Response to Question 11.4

See the response to Question 11.2 for a description of the methodology for evaluating Monticello SRV piping fatigue. The basis for developing R factors used to determine maximum equivalent full stress cycles is derived from the Class 2 piping thermal fatigue techniques defined in Section NC-3611.2(e)(3) of the Code. The R factors for individual dynamic cyclic loadings also take into account consideration of loading characteristics such as frequency, time-history, and random phasing of load components.

Question 11.5

Provide the magnitudes of the dynamic load factors used in Tables 5-2.2-5 and 5-2.2-6 of the PUA report and the justification.

Response to Question 11.5

The dynamic load factors (DLF's) included in the loads specified in Tables 5-2.2-5 and 5-2.2-6 of the PUAR are summarized in Table 11.5-1.

The loading functions for water jet impingement loads and T-quencher endcap thrust loads are defined as rectangular pulse loadings. The maximum DLF specified by standard structural dynamics techniques for this type of load function is 2.0.

The DLF's for SRV air bubble drag loads were determined using Monticello in-plant test data as permitted by NUREG-0661. The criteria state that actual measured pressure waveforms determined in tests may be used to develop a maximum structural amplification for resonant conditions. Using the measured Monticello pressure waveforms, a maximum DLF of 3.0 at resonant conditions was developed and is used as a factor on loads for the SRV piping, and T-quencher and supports.

Table 11.5-1

PUAR DYNAMIC LOAD FACTORS FOR SRV PIPING, T-QUENCHERS, AND T-QUENCHER SUPPORTS

LOAD TYPE	PUAR TABLE NUMBER	DYNAMIC LOAD FACTOR (DLF)
SRV water jet impingement	5-2.2-5	2.0
SRV air bubble drag	5-2.2-5	3.0
T-quencher end-cap thrust load	5-2.2-6	2.0

Question 11.6

Provide the results of the analysis of bolted or welded connections associated with the SRV piping.

Response to Question 11.6

The specific tables in the PUAR which contain analysis results for wetwell SRV piping major support connections and welds are shown in Table 11.6-1. The referenced tables show that SRV piping wetwell support connection stresses are within allowable limits.

Table 11.6-1

PUAR TABLE REFERENCES FOR WETWELL SRV PIPING SUPPORTS, AND BOLTED AND WELDED CONNECTIONS

SUPPORT CONNECTION/WELD STRESS	PUAR TABLE NUMBER
Vent Line-SRV Piping Penetration and Welds	3-2.5-6
SRV Piping Support and Ring Girder Connections	5-2.5-6
Ramshead and T-quencher Arm Supports and Welds	5-2.5-6

Question 12.1

Provide justification for the method of lumping additional fluid masses along the ring girder, submerged length of the SRV piping, T-quencher, and supports as indicated in the PUA report.

Response to Question 12.1

The hydrodynamic masses used for evaluating submerged structures are calculated using the relationships contained in PUAR Table 1-4.1-1 which are taken from LDR Table 4.3.4-1 (Reference 12.1-1). For the SRV piping, T-quencher arms, and supports the hydrodynamic mass equations for a circular cylinder were used.

Reference 12.1-1 - General Electric Report NEDO-21888, Revision 2, "Mark I Containment Program Load Definition Report," dated December 1981.

Question 12.2

Provide justification for not considering the loads indicated in Table 1 which are required in the analysis according to NUREG-0661.

Response to Question 12.2

All loads specified by NUREG-0661 were addressed in the PUAR. The loads identified in Table 1 which are not included in Table 1-4.3-1 of the PUAR can be categorized as being negligible, not applicable to the Monticello plant, or are considered in the analysis. The loads circled in Table 1 are discussed in the paragraphs which follow.

4.3.5 Froth Impingement. The froth impingement loads on the torus shell are negligible as indicated in LDR Section 4.3.5.1. The torus support system will also have negligible effects due to the froth impingement. SRV piping does not experience any froth loads because they are out of Regions I and II froth boundaries.

4.3.8 LOCA Bubble Drag. The vent header support columns, downcomer longitudinal bracings, downcomer bracings, and ring girder are the structures above the bottom of the downcomers and below the normal water level. The LOCA

bubble drag loads on these structures are contained in PUAR Tables 3-2.2-7, 3-2.2-9, and 2-2.2-4.

4.5.3 Chugging Vent System Loads. The chugging loads on the main vent and vent header were considered in the analysis and are contained in PUAR Table 3-2.2-20.

5.2.5 T-quencher Air Bubble Drag. The SRV air bubble drag loads on these structures were considered in the PUAR. The SRV air bubble drag loads on the downcomers are given in PUAR Table 3-2.2-26. The SRV air bubble drag loads on the T-quencher and the SRV piping are given in PUAR Table 5-2.2-3, and the SRV air bubble drag loads on the T-quencher supports and vent header support columns are given in PUAR Tables 5-2.2-1 and 3-2.2-25, respectively.

5.2.6 Thrust Loads on T-quencher Arms. The thrust loads on T-quencher arms are given in PUAR Table 5-2.2-2.

5.2.7 SRVDL Environmental Temperatures. The SRV discharge line environmental temperature loads are discussed on page 5-2.22 of the PUAR.

5.3 Ramshead Loads. Ramshead loads are not applicable for Monticello since the SRV lines are equipped with T-quencher discharge devices rather than ramsheads.

Table 1

STRUCTURAL LOADING

LEGEND

X - LOADS REQUIRED BY NUREG 0661 (1) WHICH ARE INCLUDED IN PUAR

⊗ - LOADS REQUIRED BY NUREG 0661 (1) NOT INCLUDED IN PUAR

LOADS	STRUCTURES						OTHER WETWELL INTERIOR STRUCTURES		
	TORUS SHELL	TORUS SUPPORT SYSTEMS	MAIN VENTS	VENT HEADER	DOWNCOMERS	SRV PIPING	ABOVE NORMAL WATER LEVEL	ABOVE BOTTOM OF DOWNCOMER AND BELOW NORMAL WATER LEVEL	BELOW BOTTOM OF DOWNCOMER
4.1 CONTAINMENT PRESSURE AND TEMPERATURE	X	X	X	X	X	X	X	X	X
4.2 VENT SYSTEM THRUST LOADS			X	X	X				
4.3 POOL SWELL									
4.3.1 TORUS NET VERTICAL LOADS	X	X							
4.3.2 TORUS SHELL PRESSURE HISTORIES	X	X							
4.3.3 VENT SYSTEM IMPACT AND DRAG			X	X	X				
4.3.4 IMPACT AND DRAG ON OTHER STRUCTURES			X			X	X		
4.3.5 FROTH IMPINGEMENT	⊗	⊗	X			⊗	X		
4.3.6 POOL FALLBACK						X	X	X	
4.3.7 LOCA JET						X			X
4.3.8 LOCA BUBBLE DRAG						X		⊗	X
4.4 CONDENSATION OSCILLATION									
4.4.1 TORUS SHELL LOADS	X	X							
4.4.2 LOADS ON SUBMERGED STRUCTURES						X		X	X
4.4.3 LATERAL LOADS ON DOWNCOMERS				X	X				
4.4.4 VENT SYSTEM LOADS			X	X					
4.5 CHUGGING									
4.5.1 TORUS SHELL LOADS	X	X							
4.5.2 LOADS ON SUBMERGED STRUCTURES						X		X	X
4.5.3 LATERAL LOADS ON DOWNCOMERS				X	X				
4.5.4 VENT SYSTEM LOADS			⊗	⊗					
5.2 T-QUENCHER LOADS									
5.2.1 DISCHARGE LINE CLEARING						X			
5.2.2 TORUS SHELL PRESSURES	X	X							
5.2.4 JET LOADS ON SUBMERGED STRUCTURES					X	X		X	X
5.2.5 AIR BUBBLE DRAG					⊗	⊗		⊗	⊗
5.3.6 THRUST LOADS ON T-QUENCHER ARMS						⊗			
5.2.7 SRVDL ENVIRONMENTAL TEMPERATURE						⊗			
5.3 RAMSHEAD LOADS									
5.3.1 DISCHARGE LINE CLEARING						⊗			
5.3.2 TORUS SHELL PRESSURES	⊗	⊗							
5.3.4 JET LOADS ON SUBMERGED STRUCTURES					⊗	⊗		⊗	⊗
5.3.5 AIR BUBBLE DRAG					⊗	⊗		⊗	⊗
5.3.6 SRVDL ENVIRONMENTAL TEMPURATURE						⊗			

nutech ENGINEERS

Question 12.3

Provide information on the analysis of the attachment welds of regions connecting the internal structures to the torus shell, indicating whether the criteria requirements have been satisfied.

Response to Question 12.3

The internal structure attachment welds to the torus shell have been evaluated in accordance with the criteria requirements. The attached Table 12.3-1 shows the most highly stressed catwalk and monorail support attachment welds to the torus shell and ring girder. The load combinations for which the welds are evaluated are presented in PUAR Table 4-2.2-2. The welds are evaluated using the ASME Code criteria contained in Subsection NE for Class MC components. As can be seen from the attached table, the internal structure attachment weld stresses are within allowable limits.

Table 12.3-1

CATWALK AND MONORAIL SUPPORT WELD STRESSES

ITEM	CALCULATED STRESS (ksi)	ALLOWABLE STRESS (ksi)	CALCULATED / ALLOWABLE
Catwalk Pad Plates Weld	2.49	22.91	0.11
Monorail Support Bracket to Ring Girder Weld	22.32	22.91	0.97

Question 13

PUAR Section 2.2.2.1 (Page 2.2-32), AC Sections 2.3 and 2.4. Additional information is required concerning the torus shell pressures presented in Table 2-2.2-3 on page 2-2.49 of the PUAR. Provide the details of a specific torus shell pressure calculation at the two times specified in the table for a typical longitudinal location as a function of circumferential location (e.g., $Z/\ell = 0$, $\theta = 180$, 150, 120, and 90 degrees). The following information should be included as part of the response with and without the margins imposed by NUREG-0661.

(a) Net torus vertical load history.

(b) Average submerged pressure history.

(c) Torus airspace pressure history.

Illustrate how these pressure histories are used in conjunction with the Load Definition Report (LDR) multipliers to arrive at the values presented in the table.

Response to Question 13

As discussed in the response to Question 14, the transient structural analysis of the Monticello suppression chamber for pool swell loads is performed using net pressure loadings which are obtained by subtracting the airspace pressure transient from

the submerged pressure transient. The net pressures used in the structural analysis include the margins imposed by NUREG-0661. PUAR Figure 2-2.2-8 shows an example of a resulting net pressure transient used in the analysis.

The attached Table 13-1 provides additional information to clarify PUAR Table 2-2.2-3. Table 13-1 shows the torus shell pressure values used in the Monticello structural analysis which were calculated in accordance with NUREG-0661 requirements. The bases for the values in Table 13-1 and PUAR Table 2-2.2-3 are described in the following paragraphs.

The sample pressure values shown in PUAR Table 2-2.2-3 were obtained by taking the net pressure loads used in the structural analysis of the suppression chamber including the NUREG-0661 margins, and adding the torus airspace pressures obtained from the PULD curves with NUREG-0661 margins. For ease of review, the pressures shown in Table 2-2.2-3 were reported at the same longitudinal locations as the locations at which the Load Definition Report (LDR) longitudinal multipliers are specified. The LDR specifies values at five Z/ℓ locations for calculating longitudinal multipliers. Intermediate values used in the Monticello analysis are obtained by interpolating and enveloping the LDR values. Each longitudinal multiplier is conservatively applied over a range of Z/ℓ values.

Table 13-1 shows torus shell pressure components which include all the NUREG-0661 margins. Table 13-1 also shows locations at which the LDR longitudinal multipliers were obtained and the range over which each multiplier was applied. A description of how the values in Table 13-1 were obtained is provided in the following paragraphs.

The average submerged pressure time-history, the torus airspace pressure time-history, and the net torus vertical load time-history without the margins imposed by NUREG-0661 are given in Monticello PULD Figures MC 4.3.2-1, MC 4.3.2-3 and MC 4.3.1-1, respectively. The pressure values at the time of peak download (t = 0.248 sec) and at the time of peak upload (t = 0.525 sec) are given in Table 13-2. The net torus load pressures shown in Table 13-2 are calculated by subtracting the airspace pressure values from the average submerged pressures.

The average submerged pressures and the torus airspace pressures with the NUREG-0661 margins applied are provided in the attached Table 13-3. For the download, a margin of 12.9% of the net torus vertical pressure was conservatively applied. For the upload, a margin of 21.5% was applied as required by NUREG-0661. The download margin is applied to the average submerged pressure curve during that portion of the time-history when a net download is acting on the torus, while the upload factor is applied to the torus airspace pressure curve during that portion of the time-history when a net upload is acting on the torus.

Torus shell pressures for a typical longitudinal location (Z/ℓ = 0.552) are shown in Table 13-4. This table shows local pressures at each circumferential location are calculated using the relationship $P_{loc} = (P_{avg})'_M \times M_Z \times M_\theta$. The pressures $(P_{avg})'_M$ are obtained by subtracting the airspace pressure from the average submerged pressure, as shown in Table 13-3. The pressure values shown in Table 13-4 are the same as in Table 13-1.

Table 13-1 provides additional information to clarify PUAR Table 2-2.2-3 and shows the net pressures used in the structural analysis, which includes the margins imposed by NUREG-0661.

Table 13-1

TORUS SHELL PRESSURES DUE TO POOL SWELL AT KEY TIMES AND SELECTED LOCATIONS

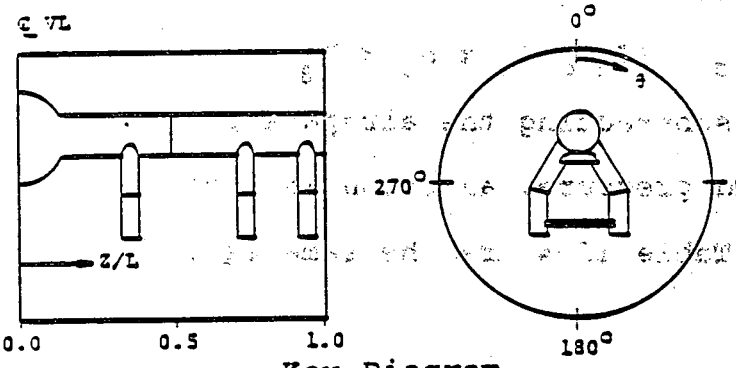

Key Diagram

LONGITUDINAL LOCATION (Z/ℓ)		CIRCUMFERENTIAL LOCATION (θ) (deg)	TORUS SHELL PRESSURE (psi)	
LONGITUDINAL FACTOR LOCATION	APPLICABLE RANGE		PEAK DOWNLOAD (t=0.248 sec)	PEAK UPLOAD (t=0.525 sec)
	0.000 - .361	180	14.6	7.2
MAXIMUM AT	0.000 - .361	150,210	13.2	6.9
0.0 OR 0.361	0.000 - .361	120,240	7.9	4.9
	0.000 - .361	0-90,270-0	0.4	14.6
	0.361 - .500	180	15.9	7.9
FACTOR	0.361 - .500	150,210	14.4	7.7
INTERPOLATED	0.361 - .500	120,240	8.6	5.9
AT 0.50	0.361 - .500	0-90,270-0	0.4	14.6
	0.500 - .640	180	16.4	7.9
0.552	0.500 - .640	150,210	14.8	7.7
	0.500 - .640	120,240	8.9	5.9
	0.500 - .640	0-90,270-0	0.4	14.6
	0.640 - .810	180	17.1	8.1
FACTOR	0.640 - .810	150,210	15.4	7.9
INTERPOLATED	0.640 - .810	120,240	9.3	6.1
AT 0.724	0.640 - .810	0-90,270-0	0.4	14.6
	0.810 - 1.0	180	17.9	8.2
0.895	0.810 - 1.0	150,210	16.1	8.0
	0.810 - 1.0	120,240	9.6	6.3
	0.810 - 1.0	0-90,270-0	0.4	14.6

Table 13-2

PRESSURES AT TIME OF PEAK DOWNLOAD AND PEAK UPLOAD

WITHOUT NUREG-0661 MARGINS

TIME	AVERAGE SUBMERGED PRESSURE P_{avg} (psi)	AIRSPACE PRESSURE P_a (psi)	NET TORUS LOAD PRESSURE P_{net} (psi)
PEAK DOWNLOAD (t = 0.248 sec)	11.7	0.4	11.3
PEAK UPLOAD (t = 0.525 sec)	7.2	13.3	-6.1

Table 13-3

PRESSURES AT TIME OF PEAK DOWNLOAD AND PEAK UPLOAD WITH NUREG-0661 MARGINS

TIME	AVERAGE SUBMERGED PRESSURE $(P_{avg})_M$ (psi)	AIRSPACE PRESSURE $(P_a)_M$ (psi)	AVERAGE PRESSURE FOR CALCULATING LOCAL PRESSURES (psi) $(P_{avg})'_M = (P_{avg})_M -$ $(P_a)_M$
PEAK DOWNLOAD (1) (t = 0.248 sec)	11.7 + 0.129 x 11.3 = 13.2	0.4	12.8
PEAK UPLOAD (2) (t = 0.525 sec)	7.2	13.3 + 6.1 x 0.215 = 14.6	-7.4

(1) AT THE TIME OF PEAK DOWNLOAD (t = 0.248 sec)

$$(P_{avg})_M = P_{avg} + 0.129 \times P_{net}$$

(2) AT THE TIME OF PEAK UPLOAD (t = 0.525 sec)

$$(P_a)_M = P_a + 0.215 \times P_{net}$$

Table 13-4

TORUS SHELL PRESSURE CALCULATIONS DUE TO POOL SWELL

FOR A TYPICAL LONGITUDINAL LOCATION ($Z/\ell = 0.552$)

CIRCUMFERENTIAL LOCATION (θ) (deg) (1)	TIME (sec)	FACTOR M_Z (2)	FACTOR M_θ (2)	LOCAL PRESSURES (psi) $P_{loc} = (P_{avg})' M \times M_Z \times M_\theta$	LOCAL PRESSURES PLUS AIRSPACE PRESSURE (psi)
180	0.248	1.040	1.205	16.0	16.4
180	0.525	0.996	0.908	-6.7	7.9
150,210	0.248	1.040	1.083	14.4	14.8
150,210	0.525	0.996	0.940	-6.9	7.7
120,240	0.248	1.040	0.638	8.5	8.9
120,240	0.525	0.996	1.186	-8.7	5.9
0-90, 270-0	0.248	-	-	0.4	0.4
0-90, 270-0	0.525	-	-	14.6	14.6

(1) FOR CIRCUMFERENTIAL LOCATIONS, SEE PUAR TABLE 2-2.2-3.

(2) THESE FACTORS ARE TAKEN FROM THE LDR, TABLE 4.3.2.1.

Question 14

PUAR Section 2-2.2.1 (Page 2-2.32), AC Sections 2.3 and 2.4. Describe in detail how the peak download and peak upload values presented in Figure 2-2.2-8 on page 2-2.65 of the PUAR were determined. Provide any additional information required to duplicate these results which has not already been requested above. In addition, describe how this transient is used in the dynamic analysis of the torus shell loads.

Response to Question 14

The values presented in PUAR Figure 2-2.2-8 are for the mitered joint location ($Z/\ell = 0.5$) and at bottom dead center ($\theta = 180^0$). For a given location, the maximum and minimum values are obtained at the times of peak download and upload (t = 0.248 and 0.525 sec) by subtracting airspace pressures from the local submerged shell pressures. For example, at $Z/\ell = 0.552$ and $\theta = 180^0$ (See Table 13-4 in the response to Question 13):

Peak Download = 16.4 - 0.4 = 16.0 psi

Peak Upload = 7.9 - 14.6 = -6.7 psi

The factor M_z at $Z/\ell = 0.552$ is conservatively applied over the range of Z/ℓ values from 0.5 to 0.64. Therefore, the local pressure values at $Z/\ell = 0.5$ shown in PUAR Figure 2-2.2-8 are the same as the values at $Z/\ell = 0.552$.

Pressure time-histories, such as the one shown in PUAR Figure 2-2.2-8, are calculated at 50 submerged torus shell locations in a 1/16 segment of the torus shell. These time-histories are used in performing a transient dynamic analysis of the torus using the methods discussed in Section 2-2.4.1 of the PUAR. The airspace pressure with the NUREG-0661 margin is applied statically to the entire torus shell and added to the dynamic response to obtain the total response of the suppression chamber due to pool swell.